Mathematical study of a new coupled electro-thermo radiofrequency model of cardiac tissue

Mostafa Bendahmane, Youssef Ouakrim, Yassine Ouzrour, Mohamed Zagour

Mathematical study of a new coupled electro-thermo radiofrequency model of cardiac tissue

Mostafa Bendahmane[a,*], Youssef Ouakrim[b], Yassine Ouzrour[b] and Mohamed Zagour[c]

[a]*Institut de Mathématiques de Bordeaux and INRIA-Carmen Bordeaux Sud-Ouest, Université de Bordeaux, Bordeaux, France*

[b]*Laboratoire de Mathématiques, Modélisation et Physique Appliquée, Ecole Normale Supérieure de Fès, Université Sidi Mohamed Ben Abdellah, Maroc.*

[c]*Euromed University of Fes, UEMF, Morocco*

ARTICLE INFO

Keywords:
Bio-heat equation
Navier–Stokes equation
Thermistor problem
Radiofrequency ablation
Cardiac tissue
Finite element method.

ABSTRACT

This paper presents a nonlinear reaction-diffusion-fluid system that simulates radiofrequency ablation within cardiac tissue. The model conveys the dynamic evolution of temperature and electric potential in both the fluid and solid regions, along with the evolution of velocity within the solid region. By formulating the system that describes the phenomena across the entire domain, encompassing both solid and fluid phases, we proceed to an analysis of well-posedness, considering a broad class of right-hand side terms. The system involves parameters such as heat conductivity, kinematic viscosity, and electrical conductivity, all of which exhibit nonlinearity contingent upon the temperature variable. The mathematical analysis extends to establishing the existence of a global solution, employing the Faedo–Galerkin method in a three-dimensional space. To enhance the practical applicability of our theoretical results, we complement our study with a series of numerical experiments. We implement the discrete system using the finite element method for spatial discretization and an Euler scheme for temporal discretization. Nonlinear parameters are linearized through decoupling systems, as introduced in our continuous analysis. These experiments are conducted to demonstrate and validate the theoretical findings we have established.

1. Introduction and problem statement

1.1. Background

The paper introduces a mathematical model for tracking the evolution of an invasive medical technique that is widely employed across various medical disciplines, specifically Radiofrequency Ablation (RFA). Our goal is to improve the applicability and efficiency of this technique, particularly in the treatment of conditions like cardiac arrhythmia and the ablation of tumors located in different regions of the body. The RFA technique is characterized by its exceptional precision, high effectiveness, and low mortality rates. RFA has evolved into a widely accepted and highly effective treatment for a variety of cardiac arrhythmias, including ventricular arrhythmias, atrial fibrillation, and atrial tachycardia, among others. The operation of this treatment technique is based on the application of high-frequency electrical current within specific myocardial regions (see Figure 1). This process leads to the generation of elevated temperatures (typically exceeding 50 °C) within the cardiac tissue, resulting in cell death. RFA procedures are mathematically represented through a thermistor problem, which simulates the heating of a conductive material by inducing electric current at a specific boundary region for a defined time period. This model is formulated as a coupled system of nonlinear partial differential equations (PDEs), specifically consisting of the heat equation with Joule heating as the heat source and the current conservation equation with temperature-dependent electrical conductivity.

The need to control the results of RFA experiments has driven various research efforts. For instance, there has been a focus on predicting tissue temperatures to provide real-time guidance during the process, as established in [24, 37]. These investigations have primarily centered on optimal control and inverse problems, with a specific emphasis on identifying the frequency factor and energy involved in the thermal damage function for different tissue types. In this context, we refer to the two works by Meinlschmidt et al. [29, 30], which addressed boundary condition identification problems through optimization techniques. The authors established the well-posedness and optimality conditions. A

mostafa.bendahmane@u-bordeaux.fr (M. Bendahmane); youssef.ouakrim@usmba.ac.ma (Y. Ouakrim); yassine.ouzrour@usmba.ac.ma (Y. Ouzrour); zagourmohamed@gmail.com (M. Zagour)

ORCID(s):

recent contribution by Huaman et al. [23] explores the local null controllability of the thermistor problem, considering spatially distributed control.

In the following subsections, we describe the coupled system that models the dynamics of radiofrequency ablation (RFA) treatment in the presence of a specific fluid, namely, blood. Let $T > 0$ represent the final time, and consider bounded open subsets in three-dimensional space denoted as Ω_b and Ω_{ts}. These subsets correspond respectively to the blood vessel and the cardiac tissue and possess piecewise smooth boundaries denoted by Σ_b and Σ_{ts}. For visual reference, Figure 1 illustrates the radiofrequency ablation procedure within cardiac tissue, showing an overview of different regions within the domain. The readers can consult the configuration geometry and boundaries conditions of our model in Figure 2.

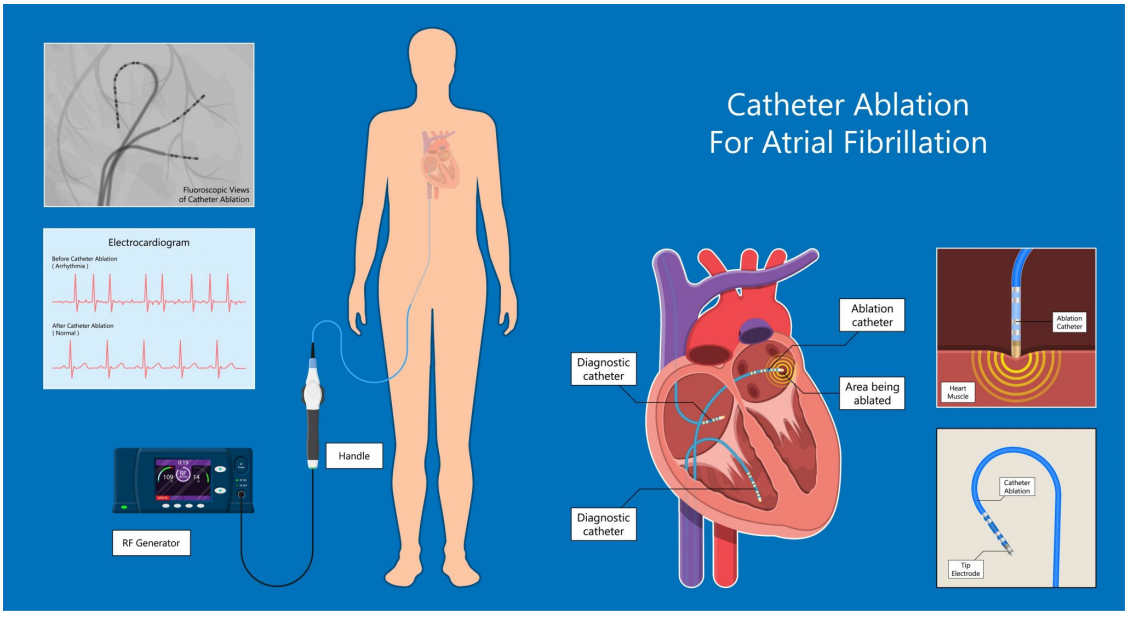

Figure 1: Illustration of radiofrequency ablation procedure within cardiac tissue, highlighting different regions in the domain. https://www.stopafib.org/procedures-for-afib/catheter-ablation/

1.2. Electrothermal field in thermistor models

RFA utilizes alternating electric currents within the radiofrequency range (450 - 500 kHz) to induce controlled thermal damage in tissues. This technique is commonly employed for the treatment of conditions such as liver, lung, and kidney tumors, varicose veins, as well as cardiac arrhythmias. During this procedure, an electrode is inserted under image guidance to precisely target and heat the tissue. When alternating electric fields are applied to resistive materials like biological tissue, two forms of heating occur; conduction losses resulting from resistive heating due to ion movement and dielectric losses caused by the rotation of molecules in the alternating electric field. However, within the frequency range below 1 MHz, dielectric losses become negligible [9].

In our model, we exclusively focus on resistive heating. The resulting electric field within the tissue can be accurately described by the Laplace equation:

$$\nabla \cdot \left(\sigma_{ts} \nabla \varphi_{ts}\right) = 0 \quad \text{in } \Omega_{T,ts} := (0,T) \times \Omega_{ts}, \tag{1}$$

where, σ_{ts} denotes the electrical conductivity of the material in Siemens per meter (S/m), and φ_{ts} represents the electric potential in Volts (V). The electric field intensity, denoted as $\mathbf{E}$ in units of Volts per meter ((V/m)), and the current density $\mathbf{J}$ in Amperes per square meter $\left(\mathrm{A/m^2}\right)$ are calculated from the following relationships: $\mathbf{E} = -\nabla\varphi$ and $\mathbf{J} = \sigma_{ts}\mathbf{E}$. The local power density responsible for tissue heating is determined by multiplying the current density $\boldsymbol{J}$ by the electric field intensity $\boldsymbol{E}$. This power density is then used to compute the temperature distribution within the tissue using the heat-transfer equation [22].

This equation accurately characterizes the situation when the ablation catheter is within the tissue, although it's important to acknowledge that the electric field might also extend into the adjacent blood vessel. As a result, both scenarios are considered simultaneously.

1.3. Bio-heat distribution

During radiofrequency ablation (RFA), electrical energy is delivered, causing a rise in temperature in both the blood vessel and the cardiac tissue surrounding the catheter. In our study we employs the Pennes equation to describe the bio-heat transfer model:

$$\rho_{1,i}\rho_{2,i}\,\theta_{t,i} - \nabla\cdot\left(\eta_i\left(\theta_i\right)\nabla\theta_i\right) = \mathcal{S}_i + \rho_{m,i} \qquad \text{in } \Omega_{T,i} := (0,T)\times\Omega_i, \qquad \text{for } i = b,\, ts, \tag{2}$$

where $\rho_{1,i}$ (kg/m^3), $\rho_{2,i}$ $(J/kg\times K)$, and η_i represent the density, specific heat, and thermal conductivity functions dependent on the media (blood vessel for $i = b$ or the tissue for $i = ts$), respectively. Recall that Ω_b and Ω_{ts} represent the tissue and blood vessel domains. The coefficient $\rho_{m,i}$ models the metabolic heat generation for $i = b, ts$. Finally, the electromagnetic heat source $\mathcal{S}_i$ (W/m^3) due to radiofrequency heating is given by:

$$\mathcal{S}_i = \sigma_i\left(\theta_i\right)|\nabla\varphi_i|^2 \qquad \text{in } \Omega_{T,i}, \qquad \text{for } i = b,\, ts. \tag{3}$$

It's important to mention that during RFA, the electromagnetic heat source ($\mathcal{S}\simeq\mathcal{O}(10^8)$) is significantly greater in magnitude compared to the metabolic heat source ($\rho_m\simeq\mathcal{O}(10^3)$). Therefore, in this work, we neglect the metabolic heat generation $\rho_{m,i}$ for $i = b, ts$. In our bio-heat model (2), the thermal and electrical conductivities of the blood and the tissue depend on the temperature of the media.

1.4. Blood flow model

The blood flow can be characterized as an incompressible Navier–Stokes fluid, governed by the following system:

$$\begin{aligned} &\rho\left(\partial_t\boldsymbol{u} + (\boldsymbol{u}\cdot\nabla)\,\boldsymbol{u}\right) - \nabla\cdot\left(\mu\left(\theta_b\right)\mathbb{D}\left(\boldsymbol{u}\right)\right) + \nabla\pi = \boldsymbol{F}, && \text{in } \Omega_{T,b},\\ &\nabla\cdot\boldsymbol{u} = 0, && \text{in } \Omega_{T,b}. \end{aligned} \tag{4}$$

Here, $\boldsymbol{u}$ represents the flow velocity, and π denotes the pressure scaled by the density ρ. The parameter μ signifies the dynamic viscosity of the blood, equivalent to $\rho\nu$, where ν is the kinematic viscosity that depends on the temperature θ_b of the blood vessel. In (4), the functions $\mathbb{D}(\boldsymbol{u}) = \frac{1}{2}\left(\nabla u + \nabla u^T\right)$ and $\boldsymbol{F}$ represents the strain rate tensor and the external force, respectively.

In the context of initial data for fluid velocity, it is essential to provide a carefully prescribed value. Typically, this velocity field should be divergence-free to be considered admissible. In many hemodynamic simulations, the actual value of this quantity is often unknown. As a result, it is frequently set to zero throughout the domain, or, in a more informed approach, it is estimated as the solution to a stationary Stokes problem. The issue of boundary conditions is of utmost significance when simulating blood flow. Extensive literature has been dedicated to addressing this topic in recent years, with comprehensive reviews available, such as in [15, 32].

1.5. Electro-thermo-fluid model

The electro-thermo-fluid model addressed in this paper is formulated as follows, summarizing all the equations described above:

$$\begin{cases} \rho\left(\partial_t \boldsymbol{u} + (\boldsymbol{u}\cdot\nabla)\,\boldsymbol{u}\right) - \nabla\cdot\left(\mu\left(\theta_b\right)\mathbb{D}\left(\boldsymbol{u}\right)\right) + \nabla\pi = \boldsymbol{F}, & \text{in } \Omega_{T,b}, \\ \nabla\cdot\boldsymbol{u} = 0, & \text{in } \Omega_{T,b}, \\ \partial_t\theta_b - \nabla\cdot\left(\eta_b\left(\theta_b\right)\nabla\theta_b\right) + \boldsymbol{u}\cdot\nabla\theta_b - \left(\sigma_b\left(\theta_b\right)\nabla\varphi_b\right)\cdot\nabla\varphi_b = 0, & \text{in } \Omega_{T,b}, \\ -\operatorname{div}\left(\sigma_b\left(\theta_b\right)\nabla\varphi_b\right) = 0, & \text{in } \Omega_{T,b}, \\ \partial_t\theta_{ts} - \nabla\cdot\left(\eta_{ts}\left(\theta_{ts}\right)\nabla\theta_{ts}\right) - \left(\sigma_{ts}\left(\theta_{ts}\right)\nabla\varphi_{ts}\right)\cdot\nabla\varphi_{ts} = 0, & \text{in } \Omega_{T,ts} \\ -\operatorname{div}\left(\sigma_{ts}\left(\theta_{ts}\right)\nabla\varphi_{ts}\right) = 0, & \text{in } \Omega_{T,ts}. \end{cases} \tag{5}$$

We complete the system (5) with the following boundary conditions

$$\begin{aligned} &\boldsymbol{u} = \boldsymbol{u}_d \ \text{ on } \Sigma_{T,b}, \\ &\theta_b = \bar{\theta} \ \text{ on } \Sigma_{T,b}^D \quad \text{and} \quad \theta_{ts} = \bar{\theta} \ \text{ on } \Sigma_{T,ts}^D, \\ &\theta_b = \theta_{ts} \ \text{ on } \Sigma_{T,7}\cup\Sigma_{T,8} \quad \text{and} \quad \left(\eta_b\left(\theta_b\right)\nabla\theta_b\right)\cdot\boldsymbol{n}_b = -\left(\eta_{ts}\left(\theta_{ts}\right)\nabla\theta_{ts}\right)\cdot\boldsymbol{n}_b \ \text{ on } \Sigma_{T,7}\cup\Sigma_{T,8}, \\ &\sigma_i\left(\theta_i\right)\nabla\varphi_i\cdot\boldsymbol{n}_b = 0 \ \text{ on } \Sigma_{T,7} \quad \text{and} \quad \varphi_i = \varphi_{i,d} \ \text{ on } \Sigma_{T,i}\setminus\Sigma_{T,7}, \end{aligned} \tag{6}$$

where $\Sigma_{T,i} := (0,T)\times\Sigma_i$ for $i = b, ts$. The initial data are

$$\begin{aligned} &\theta_i(0,\cdot) = \bar{\theta} \quad \text{on} \quad \Omega_i, \qquad \forall i = b, ts, \\ &\boldsymbol{u}(0,\cdot) = \boldsymbol{u}_0 \quad \text{on} \quad \Omega_b. \end{aligned} \tag{7}$$

Here, we divide the boundaries of blood domain Ω_b and tissue domain Ω_{ts} into regular parts Σ_i^D, Σ_i^N and Σ_8, as illustrated in Figure 2. Thus,

$$\Sigma_i := \Sigma_i^D \cup \Sigma_7 \cup \Sigma_8, \quad \Sigma_b^D := \cup_{i=0}^3 \Sigma_i, \quad \Sigma_{ts}^D := \cup_{i=4}^6 \Sigma_i,$$

$$\theta_d = \begin{cases} \theta_s & \text{on } \Sigma_{T,8}, \\ \bar{\theta} & \text{on } \Sigma_T \setminus \left(\Sigma_{T,7}\cup\Sigma_{T,8}\right), \end{cases}, \quad \varphi_{i,d} = \begin{cases} \varphi_d & \text{on } \Sigma_{T,8}, \\ 0 & \text{on } \Sigma_{T,i}\setminus\left(\Sigma_{T,7}\cup\Sigma_{T,8}\right), \end{cases}$$

$$\text{and} \qquad \boldsymbol{u}_d = \begin{cases} \boldsymbol{u}_e & \text{on } \Sigma_{T,1}\cup\Sigma_{T,3}, \\ \boldsymbol{u}_s & \text{on } \Sigma_{T,8}, \\ \boldsymbol{0} & \text{on } \Sigma_7\cup\Sigma_{T,2}. \end{cases}$$

Regarding the blood boundary conditions, we impose inlet and outlet velocity boundary conditions $\boldsymbol{u} = \boldsymbol{u}_e$ on the left and right surfaces of the blood volume ($\Sigma_{T,1}\cup\Sigma_{T,3}$). We assume that the saline irrigation flow ($\boldsymbol{u} = \boldsymbol{u}_s$ on $\Sigma_{T,8}$) serves as a velocity boundary condition applied to the area of the electrode tip. On the remaining boundary of the blood volume Σ_b (Σ_7), we apply a no-slip condition ($\boldsymbol{u} = 0$). For the thermal boundary conditions, a constant temperature $\bar{\theta} = 37°C$ is set on $\Sigma_{T,b}^D \setminus (\Sigma_{T,7}\cup\Sigma_{T,8})$ for θ_b and temperature of the saline flow is denoted by θ_s ($\theta_{ts} = \theta_b = \theta_s$ on $\Sigma_{T,8}$). On the contact surface ($\Sigma_{T,7}$) between the two media (blood and tissue), we ensure the continuity of the flux and temperature. Similarly, a constant temperature of $\theta_{ts} = 37°C$ is maintained on the remaining boundary surface of the tissue ($\Sigma_{T,4}\cup\Sigma_{T,5}\cup\Sigma_{T,6}$). In the electrical model, we enforce a zero flux boundary condition on the tissue-blood surface Σ_b^N, except on the surface of the conducting part of the RF probe ($\Sigma_{T,8}$), where $\varphi_i = \varphi_d$ for $i = b, ts$. On the remaining boundary surface of the tissue and blood, we set $\varphi_i = 0$ for $i = b, ts$.

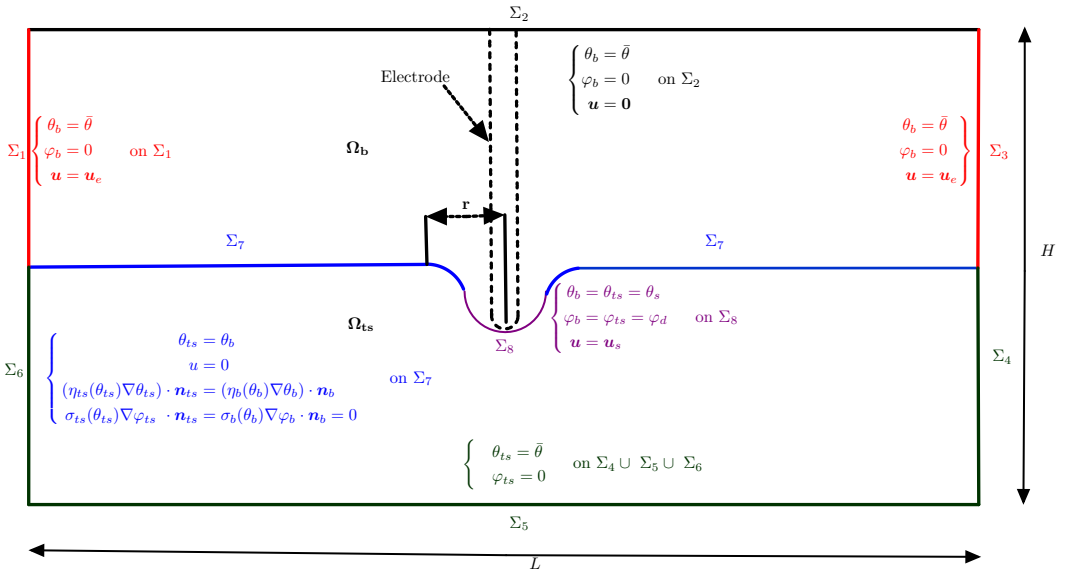

Figure 2: Configuration geometry and boundaries conditions of the model.

1.6. Contributions and related works

The mathematical study of thermistor models, particularly the heat-potential model, has been the subject of several works. For instance, in [3], the existence of a solution is established based on the maximum principle and a fixed-point argument. In [12], the existence of a weak solution over an arbitrarily large time interval is demonstrated using the Faedo–Galerkin method. In [27], the existence and uniqueness of the solution for thermistor equations were addressed without relying on non-generalized assumptions on the data. Additionally, in the case of constant thermal conductivities, the existence and uniqueness of the solution in three-dimensional space are shown, with a particular emphasis on its α-Hölder continuity, as seen in [38]. From a computational perspective, there is currently a lack of numerical analyses covering various scenarios of the model, including variations in conductivity and spatial considerations. In the context of two-dimensional space, where constant thermal conductivity is assumed, significant results were developed in [2]. In the latter, by using a mixed finite element method with a linearized semi-implicit Euler scheme, an optimal error estimate for the L^2 norm is derived while adhering to specific time-step conditions. Expanding this computational approach to higher-dimensional spaces, particularly in two and three dimensions (see [26]), time-step conditions for linearized semi-implicit methods are developed. Furthermore, optimal error estimates have been presented for a Crank-Nicolson Galerkin method concerning nonlinear thermistor equations [25], as well as for similar schemes based on backward differential formulas [17]. In order to enhance our understanding of the practical application of thermistor equations in various scenarios and dimensions, developing models that couple the thermistor system with Navier–Stokes systems presents a challenge. These results can be particularly relevant for addressing fluid dynamics during ablation, as evident in blood flow [13, 19, 28, 31, 35, 36, 39]. Some mathematical and mechanical studies of blood flow dynamics have been the subject of research, such as [14, 32].

In this paper, our primary focus is on the mathematical investigation and numerical approximation of a Thermo-Electric-Flow model. What distinguishes this model is its method of partitioning the domain into two distinct regions, representing the blood vessel and cardiac tissue, as visually depicted in Figure 2. We undertake a rigorous analysis of the electro-thermo-fluid model in three dimensions, introducing an equivalent variational formulation. Our choice of temperature-dependent electrical and thermal conductivities ensures that they satisfy the necessary conditions for the existence of solutions. By employing the Faedo–Galerkin approach and using compactness arguments, we are able to establish the existence of solutions for this model. However, it's important to note that the practical implementation of our model poses certain challenges. Specifically, the variational formulations of the heat equation encounter complications due to the quadratic terms involving electric fields in (5), denoted as $\left(\sigma_i\left(\theta_i\right)|\nabla\varphi_i|^2\right)$, where $i = b, ts$. Since we are seeking φ_i in the space $H^1\left(\Omega_i\right)$, it follows that $\sigma_i\left(\theta_i\right)|\nabla\varphi_i|^2$ is limited to $L^1\left(\Omega_i\right)$. Several approaches can be

employed to address this issue, including the selection of test functions in the variational formulations of temperatures within the space $H^1(\Omega_i) \cap L^\infty(\Omega_i)$. For further details on this approach, please refer to [10]. However, in our case, we opt for the method proposed in [4] by designating the boundary condition φ_d within the space $H^1(\Omega_i) \cap L^\infty(\Omega_i)$. The variational formulation is subsequently discretized using finite element schemes in both domains, and we utilize the domain decomposition method, particularly the Schwarz algorithm, to ensure the continuity of heat and potential equations. Temporal discretization is implemented through an Euler scheme. Finally, we present the results of numerical experiments conducted for various scenarios.

1.7. Organization of the paper

The structure of this paper is as follows. In the next section, we will introduce fundamental notations and appropriate functional spaces. Then, we will formulate the problem within a variational framework and present the existence result for the proposed model. Section 3 is dedicated to the proof of this result. We will also outline a two-dimensional numerical approach, which will be illustrated in Section 4 through various numerical experiments involving different parameter values. Lastly, Section 5 will consolidate our findings and provide insights into future perspectives.

2. Notion of solution and main result

2.1. Mathematical setting

Before presenting our results regarding weak solutions, we will first provide some preliminary materials, including relevant notations and conditions imposed on the data.

Let $\Omega = \Omega_b \cup \Omega_{ts}$ be a bounded open subset of $\mathbb{R}^N$, where $N = 3$, such that $\Omega_b \cap \Omega_{ts} = \varnothing$. The boundary of Ω is smooth and can be denoted as $\partial\Omega = \Sigma_b \cup \Sigma_{ts}$, with $\Sigma_b \cap \Sigma_{ts} = \Sigma_7 \cup \Sigma_8$ (see Figure 2). The symbol $|\Omega|$ represents the Lebesgue measure of Ω. For $i = ts, b$, we denote $H^1(\Omega_i)$ as the Sobolev space of functions $\psi : \Omega_i \to \mathbb{R}$, where $\psi \in L^2(\Omega_i)$ and $\nabla\psi \in L^2(\Omega_i; \mathbb{R}^N)$. The notation $\| \cdot \|_{L^p(\Omega_i)}$ represents the standard norm in $L^p(\Omega_i)$, with $1 \le p \le +\infty$:

$$L^p(\Omega_i) = \left\{ \psi : \Omega \longrightarrow \mathbb{R} \text{ measurable and } \int_{\Omega_i} |\psi(\mathbf{x})|^p \, d\mathbf{x} < +\infty \right\},$$

$$L^\infty(\Omega_i) = \left\{ \psi : \Omega_i \longrightarrow \mathbb{R} \text{ measurable and } \sup_{x \in \Omega_i} |\psi(\mathbf{x})| < +\infty \right\}.$$

If X is a Banach space, $a < b$, and $1 \le p \le +\infty$, the notation $L^p(a, b; X)$ represents the space of all measurable functions $\psi : (a, b) \to X$ such that $\| \psi(\cdot) \|_X$ belongs to $L^p(a, b)$. Note that $C_0^c(0, T; X)$ denotes the space of continuous functions with compact support and values in X.

To simplify mathematical formulations, we introduce the following notations, assuming that the functions $\boldsymbol{v}$, $\boldsymbol{w}$, $\boldsymbol{\psi}$, θ_i, ϕ_i, φ_i, χ_i, and S_i for $i = b, ts$ are sufficiently smooth so that the following integrals are well-defined:

$$(\boldsymbol{w}, \boldsymbol{\psi}) = \int_{\Omega_b} \boldsymbol{w} \cdot \boldsymbol{\psi} \, d\mathbf{x}, \qquad (\theta_i, S_i)_{\Gamma_i} = \int_{\Gamma_i} \theta_i \, S_i \, d\zeta,$$

$$\tilde{a}_{\boldsymbol{w}}(\boldsymbol{w}, \boldsymbol{\psi}) = \int_{\Omega_b} \mathbb{D}(\boldsymbol{w}) : \nabla\boldsymbol{\psi} \, d\mathbf{x}, \qquad d(\boldsymbol{w}, \theta_i, S_i) = \int_{\Omega_i} (\boldsymbol{w} \cdot \nabla\theta_i) \, S_i \, d\mathbf{x},$$

$$b(\boldsymbol{w}, \boldsymbol{v}, \boldsymbol{\psi}) = \int_{\Omega_b} (\boldsymbol{w}.\nabla)\boldsymbol{v} \cdot \boldsymbol{\psi} \, d\mathbf{x}, \qquad a_{\theta_i}(\phi_i; \theta_i, S_i) = \int_{\Omega_i} \eta_i(\phi_i) \nabla\theta_i \cdot \nabla S_i \, d\mathbf{x},$$

$$\tilde{a}_{\theta_i}(\theta_i, S_i) = \int_{\Omega_i} \nabla\theta_i \cdot \nabla S_i \, d\mathbf{x}, \qquad c_{\varphi_i}(\phi_i, \varphi_i, S_i) = \int_{\Omega_i} \sigma_i(\phi_i) \nabla\varphi_i \cdot \nabla\varphi_i S_i \, d\mathbf{x},$$

$$a_{\varphi_i}(\phi_i, \varphi_i, \chi_i) = \int_{\Omega_i} \sigma_i(\phi_i) \nabla\varphi_i \cdot \nabla\chi_i \, d\mathbf{x}, \qquad a_{\boldsymbol{w}}(\phi; \boldsymbol{w}, \boldsymbol{\psi}) = \int_{\Omega_b} \nu(\phi) \mathbb{D}(\boldsymbol{w}) : \nabla\boldsymbol{\psi} \, d\mathbf{x}.$$

Furthermore, in the analysis of our RF-ablation model (5), we will utilize the following vectorial spaces:

$$\mathbf{L}^2(\Omega_b) = \left(L^2(\Omega_b)\right)^3, \qquad \mathbf{H}^1(\Omega_b) = \left(H^1(\Omega_b)\right)^3, \mathbf{H}_0^1(\Omega_b) = \left(H_0^1(\Omega_b)\right)^3,$$
$$\mathcal{H}_{\mathbf{0}}^{\boldsymbol{u}} = \left\{\boldsymbol{u} \in \mathbf{H}^1(\Omega_b),\ \operatorname{div}\boldsymbol{u} = 0 \text{ and } \boldsymbol{u} = \mathbf{0} \text{ on } \Sigma_b\right\}, \quad \mathcal{L}_{\boldsymbol{b}} = \overline{\mathcal{H}_{\mathbf{0}}^{\boldsymbol{u}}}^{\mathbf{L}^2(\Omega_b)},$$
$$\mathcal{H}_0^{\theta_i} = \left\{\theta_i \in H^1(\Omega_i),\ \theta_i = 0 \text{ on } \Sigma_{T,i}^D\right\}, \text{ for } i = b, ts,$$
$$\mathcal{H}_0^{\varphi_i} = \left\{\varphi_i \in H^1(\Omega_i),\ \varphi_i = 0 \text{ on } \Sigma_{T,i}\backslash\Sigma_{T,7}\right\}, \text{ for } i = b, ts.$$

The properties of the forms $b(\cdot,\cdot,\cdot)$ are described in the following lemma, where C_1 is a positive constant (dependent on the domain) that may vary between different lines.

Lemma 2.1 (Properties of the trilinear form [16]). *The trilinear form b is continuous on* $\mathbf{H}_0^1(\Omega)\times\mathbf{H}_0^1(\Omega)\times\mathbf{H}_0^1(\Omega)$ *and satisfies:*

$$b(\boldsymbol{w},\boldsymbol{v},\boldsymbol{\psi}) + b(\boldsymbol{w},\boldsymbol{\psi},\boldsymbol{v}) = 0, \quad \forall \boldsymbol{w},\boldsymbol{v},\boldsymbol{\psi} \in \mathcal{H}_{\mathbf{0}}^{\boldsymbol{u}},$$
$$b(\boldsymbol{w},\boldsymbol{v},\boldsymbol{v}) = 0, \quad \forall \boldsymbol{w},\boldsymbol{v} \in \mathcal{H}_{\mathbf{0}}^{\boldsymbol{u}}.$$

Moreover, for all $\boldsymbol{w},\boldsymbol{v},\boldsymbol{\psi} \in \mathcal{H}_{\mathbf{0}}^{\boldsymbol{u}}$, *we have*

$$|b(\boldsymbol{w},\boldsymbol{v},\boldsymbol{\psi})| \le C_1 \|\boldsymbol{w}\|_{L^2}^{1/4}\|\boldsymbol{w}\|_{H^1}^{3/4}\|\boldsymbol{v}\|_{L^2}^{1/4}\|\boldsymbol{v}\|_{H^1}^{3/4}\|\boldsymbol{\psi}\|_{H^1}.$$

For all $\boldsymbol{w},\boldsymbol{v} \in \mathcal{H}_{\mathbf{0}}^{\boldsymbol{u}}$ we denote as $B(\boldsymbol{w},\boldsymbol{v}) \in \left(\mathcal{H}_{\mathbf{0}}^{\boldsymbol{u}}\right)'$ the bilinear form on $\mathcal{H}_{\mathbf{0}}^{\boldsymbol{u}}\times\mathcal{H}_{\mathbf{0}}^{\boldsymbol{u}}$ defined by

$$\langle B(\boldsymbol{w},\boldsymbol{v}),\boldsymbol{\psi}\rangle_{(\mathcal{H}_{\mathbf{0}}^{\boldsymbol{u}})',\mathcal{H}_{\mathbf{0}}^{\boldsymbol{u}}} = b(\boldsymbol{w},\boldsymbol{v},\boldsymbol{\psi}).$$

Then, by Lemma 2.1, it is clear that the map B is continuous from $\mathcal{H}_{\mathbf{0}}^{\boldsymbol{u}}\times\mathcal{H}_{\mathbf{0}}^{\boldsymbol{u}}$ into $(\mathcal{H}_{\mathbf{0}}^{\boldsymbol{u}})'$ and that we have

$$\|B(\boldsymbol{w},\boldsymbol{w})\|_{(\mathcal{H}_{\mathbf{0}}^{\boldsymbol{u}})'} \le C_1\|\boldsymbol{w}\|_{L^2}^{1/2}\|\boldsymbol{w}\|_{H^1}^{3/2}, \quad \forall \boldsymbol{w} \in \mathcal{H}_{\mathbf{0}}^{\boldsymbol{u}}. \tag{8}$$

2.2. Variational formulation

Before presenting our main result, we make several assumptions about the parameters and data of the model (5)-(7). Without further references, we assume the following assumptions:
Firstly, we assume that the functions μ, σ_i, and η_i are positive, bounded, and continuous with respect to the temperature

$$\begin{aligned} &0 < \underline{\nu} \le \nu(\xi) \le \overline{\nu} < +\infty && \forall \xi \in \mathbb{R}, \\ &0 < \underline{\sigma_i} \le \sigma_i(\xi) \le \overline{\sigma}_i < +\infty && \forall \xi \in \mathbb{R} \text{ and } i = b, ts, \\ &0 < \underline{\eta_i} \le \eta_i(\xi) \le \overline{\eta}_i < +\infty && \forall \xi \in \mathbb{R} \text{ and } i = b, ts, \end{aligned} \tag{9}$$

where $\underline{\nu}$, $\overline{\nu}$, $\underline{\sigma_i}$, $\overline{\sigma}_i$, $\underline{\eta_i}$ and $\overline{\eta}_i$ are positive constants.
In addition, with respect to the boundary conditions of (6), we use the notations $\boldsymbol{u}_d$, θ_d, and $\varphi_{i,d}$, and we also denote their trace extensions by the same notations. Then, we assume the following conditions:

$$\begin{aligned} &\boldsymbol{u}_d \in L^4\left(0,T;\mathbf{H}^1(\Omega_b)\right), \partial_t\boldsymbol{u}_d \in L^2\left(0,T;\left(\mathbf{H}^1(\Omega_b)\right)'\right), \quad \text{such that } \operatorname{div}\boldsymbol{u}_d = 0 \text{ in } \Omega, \\ &\theta_d \in L^2\left(0,T;H^1(\Omega_b)\cup H^1(\Omega_{ts})\right), \partial_t\theta_d \in L^2\left(0,T;\left(H^1(\Omega_b)\right)'\cup\left(H^1(\Omega_{ts})\right)'\right), \\ &\varphi_{i,d} \in L^\infty\left(0,T;H^1(\Omega_i)\cap L^\infty(\Omega_i)\right), \qquad \forall i = b, ts. \end{aligned} \tag{10}$$

The initial conditions of the temperatures and velocity on the boundary, $\theta_{d,0} := \theta_d(0,\cdot)$ and $\boldsymbol{u}_{d,0} := \boldsymbol{u}_d(0,\cdot)$, belong to $L^2(\Omega_b)\cup L^2(\Omega_{ts})$ and $\mathbf{L}^2(\Omega_b)$, respectively.
Finally, the assumptions for the rest of the data are as follows:

$$\boldsymbol{u}_0 \in \mathbf{L}^2(\Omega_b), \quad \theta_{i,0} \in L^2(\Omega_i) \text{ for } i = b, ts \quad \text{and} \quad \boldsymbol{F} \in L^2(\Omega_{T,b}). \tag{11}$$

Now we define what we mean by a weak solution of our system (5)-(7). We also supply our main existing result.

Definition 2.1. *We say that* $\left(\boldsymbol{u}, \theta_b, \theta_{ts}, \varphi_b, \varphi_{ts}\right)$ *is a weak solution to System (5), (6) and (7), if*

$$\begin{aligned}
&\boldsymbol{u}-\boldsymbol{u}_d \in L^{\infty}\left(0,T;\mathcal{L}_{\boldsymbol{b}}\right)\cap L^2\left(0,T;\mathcal{H}_{\boldsymbol{0}}^{\boldsymbol{u}}\right),\ \ \partial_t\boldsymbol{u}\in L^1\left(0,T;\left(\mathcal{H}_{\boldsymbol{0}}^{\boldsymbol{u}}\right)'\right),\\
&\theta_i-\theta_d\in L^{\infty}\left(0,T;L^2\left(\Omega_i\right)\right)\cap L^2\left(0,T;\mathcal{H}_0^{\theta_i}\right),\ \ \partial_t\theta_i\in L^1\left(0,T;\left(\mathcal{H}_0^{\theta_i}\right)'\right),\quad \text{for } i=b,ts\\
&\varphi_i-\varphi_{i,d}\in L^2\left(0,T;\mathcal{H}_0^{\varphi_i}\right)\cap L^{\infty}\left(0,T;L^{\infty}\left(\Omega_i\right)\right),\quad \text{for } i=b,ts
\end{aligned}$$

and the following identities hold

$$\begin{aligned}
&\int_0^T\langle\partial_t\boldsymbol{u},\boldsymbol{\psi}\rangle\ dt+\int_0^T a_{\boldsymbol{u}}\left(\theta_b;\boldsymbol{u},\boldsymbol{\psi}\right)\ dt+\int_0^T b\left(\boldsymbol{u},\boldsymbol{u},\boldsymbol{\psi}\right)\ dt-\int_0^T\left(\boldsymbol{F},\boldsymbol{\psi}\right)\ dt=0,\\
&\sum_{i=b,ts}\int_0^T\langle\partial_t\theta_i,S_i\rangle\ dt+\sum_{i=b,ts}\int_0^T a_{\theta_i}\left(\theta_i;\theta_i,S_i\right)\ dt+\int_0^T d\left(\boldsymbol{u},\theta_b,S_b\right)\ dt-\sum_{i=b,ts}\int_0^T c_{\varphi_i}\left(\theta_i,\varphi_i,S_i\right)\ dt=0,\\
&\sum_{i=b,ts}\int_0^T a_{\varphi_i}\left(\theta_i;\varphi_i,\phi_i\right)\ dt=0,
\end{aligned}\tag{12}$$

for all test functions $\boldsymbol{\psi}\in D\left([0,T);\mathcal{H}_{\boldsymbol{0}}^{\boldsymbol{u}}\right)$, $S_i\in D\left([0,T);\mathcal{H}_{\boldsymbol{0}}^{\theta_i}\right)$ *and* $\phi_i\in D\left([0,T);\mathcal{H}_0^{\varphi_i}\right)$, *for* $i=b,ts$, *with* $S_b=S_{ts}$ *on* $\Sigma_{T,7}\cup\Sigma_{T,8}$ *and*

$$\boldsymbol{u}(0,\boldsymbol{x})=\boldsymbol{u}_0(\boldsymbol{x})\quad \text{in } \Omega,\tag{13}$$

$$\theta_i(0,\boldsymbol{x})=\theta_{i,0}(\boldsymbol{x})\quad \text{in } \Omega,\quad \text{for } i=b,ts.\tag{14}$$

It is significant to highlight that variational formulations of the heat equations are not as straightforward as those of the Navier–Stokes system and the elliptic equations. While there is no difficulty in writing the convection term $d\left(\boldsymbol{u},\theta_b,\cdot\right)=\boldsymbol{u}.\nabla\theta_b$ in a variational sense, this term can be tested by a function in $\mathcal{H}_0^{\theta_b}\subset H^1\hookrightarrow L^4\left(\Omega_b\right)$. Since we seek the temperature θ_b in $\mathcal{H}_0^{\theta_i}$ and the velocity in $\mathcal{H}_{\boldsymbol{0}}^{\boldsymbol{u}}\subset\boldsymbol{H}^1\hookrightarrow\boldsymbol{L}^4\left(\Omega_b\right)$. However, the quadratic terms $\sigma_i\left(\theta_i\right)|\nabla\varphi_i|^2$, $i=b,ts$, cannot be tested by functions in $\mathcal{H}_0^{\theta_i}$ since we are looking for the potentials φ_i in $\mathcal{H}_0^{\varphi_i}$, as this term belongs to $L^1\left(\Omega_i\right)$. There are different methods to choose suitable function spaces. For example, we can take the test functions in the space $\mathcal{H}_0^{\theta_i}\cap L^{\infty}\left(\Omega_i\right)$ [10, 34]. Alternatively, if we set the boundary condition of the potential φ_d in the space $H^{1/2}\left(\Sigma_i\right)\cap L^{\infty}\left(\Sigma_i\right)$, we can choose the test functions for the heat equations in $\mathcal{H}_0^{\theta_i}$. A discussion of this approach can be found in [4].

Theorem 2.1. *Assume conditions (9), (10) and (11) hold. Then the RF-ablation model (5), (6) and (7) possesses a weak solution in the sense of Definition 2.1.*

The proof of Theorem 2.1 is divided into a series of steps outlined in Section 3. In Subsection 3.1, we construct an approximate solution and demonstrate its convergence. The convergence proof relies on several uniform a priori estimates and compactness arguments, which are established in Subsection 3.2. Finally, we conclude the proof of our result in Subsection 3.3.

3. Proof of Theorem 2.1

3.1. Faedo–Galerkin approximate solutions

Let, for $i=b,ts$, $\left\{\left(\xi_\ell,\alpha_{i,\ell},\beta_{i,\ell}\right)\right\}_{\ell=1,2,\dots}\subset\mathcal{H}_{\boldsymbol{0}}^{\boldsymbol{u}}\times\mathcal{H}_0^{\theta_i}\times\mathcal{H}_0^{\varphi_i}$ be an orthonormal basis of $\mathcal{L}_{\boldsymbol{b}}\times\mathcal{H}_0^{\theta_i}\times\mathcal{H}_0^{\varphi_i}$. We set $\boldsymbol{V}^n\times X_i^n\times Y_i^n=\text{span}\left\{\left(\xi_1,\alpha_{i,1},\beta_{i,1}\right),\dots,\left(\xi_n,\alpha_{i,n},\beta_{i,n}\right)\right\}$. The approximate Faedo–Galerkin problem to be solved is then: Determine $\boldsymbol{u}^n-\boldsymbol{u}_d\in H^1\left(0,T;\mathcal{H}_{\boldsymbol{0}}^{\boldsymbol{u}}\right)$, $\theta_i^n-\theta_d\in H^1\left(0,T;\mathcal{H}_0^{\theta_i}\right)$, and $\varphi_i^n-\varphi_{i,d}\in H^1\left(0,T;\mathcal{H}_0^{\varphi_i}\right)$,

$$\begin{aligned}
&\langle\partial_t\boldsymbol{u}^n,\xi_\ell\rangle+a_{\boldsymbol{u}}\left(\theta_b^n,\boldsymbol{u}^n,\xi_\ell\right)+b\left(\boldsymbol{u}^n,\boldsymbol{u}^n,\xi_\ell\right)-\left(\boldsymbol{F}^n,\xi_\ell\right)=0,\\
&\sum_{i=b,ts}\left\langle\partial_t\theta_i^n,\alpha_{i,\ell}\right\rangle+\sum_{i=b,ts}a_{\theta_i}\left(\theta_i^n;\theta_i^n,\alpha_{i,\ell}\right)+d\left(\boldsymbol{u}^n,\theta_b^n,\alpha_{1,\ell}\right)-\sum_{i=b,ts}c_{\varphi_i^n}\left(\theta_i^n,\varphi_i^n,\alpha_{i,\ell}\right)=0,\\
&\sum_{i=b,ts}a_{\varphi_i^n}\left(\theta_i^n,\varphi_i^n,\beta_{i,\ell}\right)=0,
\end{aligned}\tag{15}$$

for $\ell = 1, \ldots, n$, where

$$\boldsymbol{u}^n = \sum_{\ell=1}^{n} \boldsymbol{u}_\ell^n \xi_\ell, \qquad \theta_j^n = \sum_{\ell=1}^{n} \theta_{i,\ell}^n \alpha_{i,\ell}, \qquad \varphi_j^n = \sum_{\ell=1}^{n} \varphi_{i,\ell}^n \beta_{i,\ell} \quad \text{for } i = b,\, ts. \tag{16}$$

The initial conditions of the ODE system are then given by

$$\begin{aligned} \boldsymbol{u}^n(0) &= \sum_{\ell=0}^{n} \boldsymbol{u}_{0,\ell} \xi_\ell, \qquad \text{where } \boldsymbol{u}_{0,\ell} = \left(\boldsymbol{u}_0, \xi_\ell\right)_{L^2}, \\ \theta_i^n(0) &= \sum_{\ell=0}^{n} \theta_{i,0,\ell} \alpha_{i,\ell}, \quad \text{where } \theta_{i,0,\ell} = \left(\theta_{i,0}, \alpha_{i,\ell}\right)_{L^2}, \end{aligned} \tag{17}$$

for $i = b, ts$. We use the following assumption for the initial conditions

$$\boldsymbol{u}_0 \in L^2\left(\Omega_b\right), \ \theta_{b,0} \in L^2\left(\Omega_b\right) \text{ and } \theta_{ts,0} \in L^2\left(\Omega_{ts}\right). \tag{18}$$

In (15) we have used a finite dimensional approximation of $\boldsymbol{F}$

$$\boldsymbol{F}^n(t,x) = \sum_{\ell=0}^{n} \left(\boldsymbol{F}, \xi_\ell\right)_{L^2}(t) \xi_\ell(\mathbf{x}).$$

Using the orthonormality of the basis, we can write (15) more explicitly as a system of ordinary differential equations:

$$\begin{aligned} &\frac{d\boldsymbol{u}_\ell^n}{dt} = -a_{\boldsymbol{u}}\left(\theta_b^n, \boldsymbol{u}^n, \xi_\ell\right) - b\left(\boldsymbol{u}^n, \boldsymbol{u}^n, \xi_\ell\right) + \left(\boldsymbol{F}^n, \xi_\ell\right) := F_{\ell,\boldsymbol{u}^n}\left(t, \left\{\boldsymbol{u}_k^n\right\}_{k=1}^n, \left\{\theta_{b,k}^n\right\}_{k=1}^n\right), \\ &\sum_{i=b,ts} \frac{d\theta_{i,\ell}^n}{dt} = -d\left(\boldsymbol{u}^n, \theta_b^n, \alpha_{1,\ell}\right) - \sum_{i=b,ts} a_{\theta_i}\left(\theta_i^n; \theta_i^n, \alpha_{i,\ell}\right) + \sum_{i=b,ts} c_{\varphi_i^n}\left(\theta_i^n, \varphi_i^n, \alpha_{i,\ell}\right) \\ &\qquad := \sum_{i=b,ts} F_{\ell,\theta_i}\left(t, \left\{\boldsymbol{u}_k^n\right\}_{k=1}^n, \left\{\theta_{b,k}^n\right\}_{k=1}^n, \left\{\theta_{ts,k}^n\right\}_{k=1}^n, \left\{\varphi_{b,k}^n\right\}_{k=1}^n \left\{\varphi_{ts,k}^n\right\}_{k=1}^n\right), \\ &\sum_{i=b,ts} a_{\varphi_i^n}\left(\theta_i^n, \varphi_i^n, \beta_{i,\ell}\right) = 0, \end{aligned} \tag{19}$$

for $i = b, ts$. From the assumptions on the data of the model, the functions $F_{\ell,\boldsymbol{u}^n}$ and F_{ℓ,θ_i} (for $i = b, ts$) are Caratheodory functions. Therefore, according to ordinary differential equation theory, functions $\left\{\boldsymbol{u}_k^n\right\}_{k=1}^n$, $\left\{\theta_{b,k}^n\right\}_{k=1}^n$, and $\left\{\theta_{ts,k}^n\right\}_{k=1}^n$, satisfying the equations, exist and are absolutely continuous. Consequently, a weak local solution exists for all $t \in (0, t_0)$ with $0 < t_0 < T$. To establish the existence of φ_i^n, we regularize the elliptic equation of φ_i^n in a manner akin to [6]. Specifically, we add the term $\varepsilon_n \sum_{i=b,ts}\left(\partial_t \varphi_i^n, \beta_{i,\ell}\right)$ to the left-hand side of the last equation in (19), where $\varepsilon_n := 1/n$. We fix the initial data as $\varphi_i^n(0) = 0$ and choosing the regularity condition of φ_d that is $\partial_t \varphi_d = 0$. Then the system involving the new unknown φ_i^n (for $i = b, ts$) becomes a well-posed ordinary differential equation problem, and solutions are defined globally on $[0, T]$. The regularity parameter ε_n tends towards 0 (as n to $+\infty$) at the end of the calculations, so to simplicity we neglect these regularity terms. Then, that the Galerkin solutions $\left(\boldsymbol{u}^n, \pi^n, \theta_b^n, \theta_{ts}^n, \varphi_b^n, \varphi_{ts}^n\right)$ satisfy the following weak formulation :

$$\begin{aligned} &\int_0^T \langle \partial_t \boldsymbol{u}^n, \boldsymbol{\psi} \rangle \ dt + \int_0^T a_{\boldsymbol{u}}\left(\theta_b^n; \boldsymbol{u}^n, \boldsymbol{\psi}\right) \ dt + \int_0^T b\left(\boldsymbol{u}^n, \boldsymbol{u}^n, \boldsymbol{\psi}\right) \ dt - \int_0^T \left(\boldsymbol{F}^n, \boldsymbol{\psi}\right) \ dt = 0, \\ &\sum_{i=b,ts} \int_0^T \left\langle \partial_t \theta_i^n, S_i \right\rangle \ dt + \sum_{i=b,ts} \int_0^T a_{\theta_i}\left(\theta_i^n; \theta_i^n, S_i\right) \ dt + \int_0^T d\left(\boldsymbol{u}^n, \theta_b^n, S_b\right) \ dt - \sum_{i=b,ts} \int_0^T c_{\varphi_i}\left(\theta_i^n, \varphi_i^n, S_i\right) \ dt = 0, \\ &\sum_{i=b,ts} \int_0^T a_{\varphi_i}\left(\theta_i^n; \varphi_i^n, \phi_i\right) \ dt = 0, \end{aligned} \tag{20}$$

for all test functions $\boldsymbol{\psi} \in D\left([0,T);\mathcal{H}_{\mathbf{0}}^{\boldsymbol{u}}\right)$, $S_i \in D\left([0,T);\mathcal{H}_{\mathbf{0}}^{\theta_i}\right)$ and $\phi_i \in D\left([0,T);\mathcal{H}_0^{\varphi_i}\right)$, for $i = b, ts$, with $S_b = S_{ts}$ on $\Sigma_{T,7} \cup \Sigma_{T,8}$.

Throughout the rest of the paper, we will always use positive constants c, $C(\cdot)$, $C(\cdot,\cdot)$, C, C_1, $C_2 \cdots$, which are not specified and which may differ from line to line.

3.2. Basic a priori estimates

To establish the global existence of the Faedo–Galerkin weak solution, we rely on a series of basic energy-type estimates as presented in the following lemma.

Lemma 3.1. *Under the above assumptions, there exists a constant $C > 0$ not depending on n such that*

$$\|\boldsymbol{u}^n\|_{L^\infty(0,T;L^2(\Omega_b))} + \|\nabla \boldsymbol{u}^n\|_{L^2(\Omega_{T,b},\mathbb{R}^3)} + \left\|\partial_t \boldsymbol{u}^n\right\|_{L^1\left(0,T;\boldsymbol{H}^{-1}(\Omega_b)\right)} \leq C, \tag{21}$$

$$\sum_{i=b,ts} \left\|\varphi_i^n\right\|_{L^\infty(\Omega_{T,i})} + \sum_{i=b,ts} \left\|\nabla \varphi_i^n\right\|_{L^2(\Omega_{T,i})} \leq C, \tag{22}$$

$$\sum_{i=b,ts} \left\|\theta_i^n\right\|_{L^\infty(0,T;L^2(\Omega_i))} + \sum_{i=b,ts} \left\|\nabla \theta_i^n\right\|_{L^2(\Omega_{T,i})} + \sum_{i=b,ts} \left\|\partial_t \theta_i^n\right\|_{L^1(0,T;H^{-1}(\Omega_i))} \leq C. \tag{23}$$

Proof. *Proof of (21).* First, we substitute $\boldsymbol{\psi} := \boldsymbol{u}^n - \boldsymbol{u}_d$ into (20). Then, we disregard the time integration and combine the resulting equations to obtain:

$$\begin{aligned}
&\frac{1}{2}\frac{d}{dt}\int_{\Omega_b} |\boldsymbol{u}^n - \boldsymbol{u}_d|^2 \, d\mathbf{x} + a_{\boldsymbol{u}}\left(\theta_b^n; \boldsymbol{u}^n - \boldsymbol{u}_d, \boldsymbol{u}^n - \boldsymbol{u}_d\right) \\
&\quad = -a_{\boldsymbol{u}}\left(\theta_b^n; \boldsymbol{u}_d, \boldsymbol{u}^n - \boldsymbol{u}_d\right) - b\left(\boldsymbol{u}^n, \boldsymbol{u}^n, \boldsymbol{u}^n - \boldsymbol{u}_d\right) + \int_{\Omega_b} \boldsymbol{F}^n \cdot \left(\boldsymbol{u}^n - \boldsymbol{u}_d\right) \, d\mathbf{x} - \int_{\Omega_b} \partial_t \boldsymbol{u}_d \left(\boldsymbol{u}^n - \boldsymbol{u}_d\right) \, d\mathbf{x} \\
&\quad := I_1 + I_2 + I_3 + I_4.
\end{aligned} \tag{24}$$

From the definition of the form a_u, it follows that

$$\begin{aligned}
|I_1| &= |-a_{\boldsymbol{u}}\left(\theta_b^n; \boldsymbol{u}_d, \boldsymbol{u}^n - \boldsymbol{u}_d\right)| \\
&\leq \overline{\nu} \|\nabla \boldsymbol{u}_d\|_{L^2} \|\nabla\left(\boldsymbol{u}^n - \boldsymbol{u}_d\right)\|_{L^2} \\
&\leq \delta \|\boldsymbol{u}^n - \boldsymbol{u}_d\|_{H^1}^2 + C\left(\delta, \overline{\nu}\right) \|\nabla \boldsymbol{u}_d\|_{L^2}^2.
\end{aligned} \tag{25}$$

Using the properties of the trilinear form b, $\operatorname{div} \boldsymbol{u}^n = 0$ and $\boldsymbol{u}^n = \boldsymbol{u}_d$ on Σ_b, we obtain

$$\begin{aligned}
-I_2 &= b\left(\boldsymbol{u}^n, \boldsymbol{u}^n, \boldsymbol{u}^n - \boldsymbol{u}_d\right) \\
&= \sum_{i,j=1}^{N} \int_{\Omega_b} \boldsymbol{u}_i^n \, \partial_{x_i} \boldsymbol{u}_j^n \left(\boldsymbol{u}_j^n - \boldsymbol{u}_{j,d}\right) \, d\mathbf{x} \\
&= -\sum_{i,j=1}^{N} \int_{\Omega_b} \partial_{x_i} \boldsymbol{u}_i^n \, \boldsymbol{u}_j^n \left(\boldsymbol{u}_j^n - \boldsymbol{u}_{j,d}\right) \, d\mathbf{x} - \sum_{i,j=1}^{N} \int_{\Omega_b} \boldsymbol{u}_i^n \, \boldsymbol{u}_j^n \, \partial_{x_i}\left(\boldsymbol{u}_j^n - \boldsymbol{u}_{j,d}\right) \, d\mathbf{x} \\
&= -\int_{\Omega_b} \operatorname{div} \boldsymbol{u}^n \, \boldsymbol{u}^n \left(\boldsymbol{u}^n - \boldsymbol{u}_d\right) \, d\mathbf{x} - \frac{1}{2}\sum_{i,j=1}^{N} \int_{\Omega_b} \boldsymbol{u}_i^n \, \partial_{x_i}\left(\boldsymbol{u}_j^n\right)^2 \, d\mathbf{x} + \sum_{i,j=1}^{N} \int_{\Omega_b} \boldsymbol{u}_i^n \, \boldsymbol{u}_j^n \, \partial_{x_i} \boldsymbol{u}_{j,d} \, d\mathbf{x} \\
&= \frac{1}{2}\int_{\Omega_b} \operatorname{div} \boldsymbol{u}^n \, |\boldsymbol{u}^n|^2 \, d\mathbf{x} - \frac{1}{2}\int_{\Sigma_b} |\boldsymbol{u}_d|^2 \, \boldsymbol{u}_d \cdot \boldsymbol{n}_b dy + \sum_{i,j=1}^{N} \int_{\Omega_b} \boldsymbol{u}_i^n \, \boldsymbol{u}_j^n \, \partial_{x_i} \boldsymbol{u}_{j,d} \, d\mathbf{x} \\
&= -\frac{1}{2}\int_{\Sigma_b} |\boldsymbol{u}_d|^2 \, \boldsymbol{u}_d \cdot \boldsymbol{n}_b \, dy + \sum_{i,j=1}^{N} \int_{\Omega_b} \boldsymbol{u}_i^n \, \boldsymbol{u}_j^n \, \partial_{x_i} \boldsymbol{u}_{j,d} \, d\mathbf{x} \\
&:= I_{21} + I_{22}.
\end{aligned}$$

Obviously, I_{21} is bounded. Let us proceed with the estimation of the term I_{22}. To begin, we can reformulate I_{22} as follows:

$$I_{22} = b\left(\boldsymbol{u}_j^n - \boldsymbol{u}_{j,d}\right) = b\left(\boldsymbol{u}_d, \boldsymbol{u}_d, \boldsymbol{u}_d\right) + b\left(\boldsymbol{u}^n - \boldsymbol{u}_d, \boldsymbol{u}_d, \boldsymbol{u}_d\right) + b\left(\boldsymbol{u}_d, \boldsymbol{u}_d, \boldsymbol{u}^n - \boldsymbol{u}_d\right) + b\left(\boldsymbol{u}^n - \boldsymbol{u}_d, \boldsymbol{u}_d, \boldsymbol{u}^n - \boldsymbol{u}_d\right).$$

Since $\boldsymbol{u}_d$ is assumed to be sufficiently regular, we have the boundedness of $b\left(\boldsymbol{u}_d, \boldsymbol{u}_d, \boldsymbol{u}_d\right)$. While the second and the third terms on the right-hand side of I_{22} can be estimated by

$$\begin{aligned} |b\left(\boldsymbol{u}^n - \boldsymbol{u}_d, \boldsymbol{u}_d, \boldsymbol{u}_d\right)| + |b\left(\boldsymbol{u}_d, \boldsymbol{u}_d, \boldsymbol{u}^n - \boldsymbol{u}_d\right)| &\leq \|\boldsymbol{u}^n - \boldsymbol{u}_d\|_{L^4} \|\nabla \boldsymbol{u}_d\|_{L^2} \|\boldsymbol{u}_d\|_{L^4} + \|\boldsymbol{u}_d\|_{L^4} \|\nabla \boldsymbol{u}_d\|_{L^2} \|\boldsymbol{u}^n - \boldsymbol{u}_d\|_{L^4} \\ &\leq c\|\boldsymbol{u}^n - \boldsymbol{u}_d\|_{H^1} \|\nabla \boldsymbol{u}_d\|_{L^2} \|\boldsymbol{u}_d\|_{L^4} + c\|\boldsymbol{u}_d\|_{L^4} \|\nabla \boldsymbol{u}_d\|_{L^2} \|\boldsymbol{u}^n - \boldsymbol{u}_d\|_{H^1} \\ &\leq \delta \|\boldsymbol{u}^n - \boldsymbol{u}_d\|_{H^1}^2 + C(\delta) \|\nabla \boldsymbol{u}_d\|_{L^2}^2 \|\boldsymbol{u}_d\|_{L^4}^2. \end{aligned}$$

Furthermore, we can apply Young's inequality with a parameter δ ($ab \leq \delta a^p + C(\delta) b^q$, where $a, b > 0$, $\delta > 0$, $1 < p, q < \infty$, and $1/p + 1/q = 1$, with $C(\delta) = (\delta p)^{-q/p} q^{-1}$) and employ the Gagliardo-Nirenberg interpolation inequality (cf. [1, Theorem 5.8]), to derive the following:

$$\|\boldsymbol{u}^n - \boldsymbol{u}_d\|_{\boldsymbol{L}^4(\Omega_b)} \leq c \|\boldsymbol{u}^n - \boldsymbol{u}_d\|_{\boldsymbol{H}^1(\Omega_b)}^{\zeta} \|\boldsymbol{u}^n - \boldsymbol{u}_d\|_{\boldsymbol{L}^2(\Omega_b)}^{1-\zeta}, \text{ for } \zeta = N/4.$$

Thus, the remaining term in I_{22} can be estimated as follows

$$\begin{aligned} |b\left(\boldsymbol{u}^n - \boldsymbol{u}_d, \boldsymbol{u}_d, \boldsymbol{u}^n - \boldsymbol{u}_d\right)| &\leq \|\boldsymbol{u}^n - \boldsymbol{u}_d\|_{L^4} \|\nabla \boldsymbol{u}_d\|_{L^2} \|\boldsymbol{u}^n - \boldsymbol{u}_d\|_{L^4} \\ &\leq c\|\boldsymbol{u}^n - \boldsymbol{u}_d\|_{L^2}^{2(1-\zeta)} \|\boldsymbol{u}^n - \boldsymbol{u}_d\|_{H^1}^{2\zeta} \|\nabla \boldsymbol{u}_d\|_{L^2} \\ &\leq \delta \|\boldsymbol{u}^n - \boldsymbol{u}_d\|_{H^1}^2 + C(\delta) \|\nabla \boldsymbol{u}_d\|_{L^2}^{\frac{1}{1-\zeta}} \|\boldsymbol{u}^n - \boldsymbol{u}_d\|_{L^2}^2. \end{aligned}$$

Then, we deduce that

$$|I_{22}| \leq \delta \|\boldsymbol{u}^n - \boldsymbol{u}_d\|_{H^1}^2 + C(\delta) \|\nabla \boldsymbol{u}_d\|_{L^2}^{\frac{1}{1-\zeta}} \|\boldsymbol{u}^n - \boldsymbol{u}_d\|_{L^2}^2.$$

This implies

$$\left|I_2\right| \leq \delta \|\boldsymbol{u}^n - \boldsymbol{u}_d\|_{H^1}^2 + C(\delta, \overline{\nu}) \|\nabla \boldsymbol{u}_d\|_{L^2}^2 + C(\delta) \|\nabla \boldsymbol{u}_d\|_{L^2}^{\frac{1}{1-\zeta}} \|\boldsymbol{u}^n - \boldsymbol{u}_d\|_{\boldsymbol{L}^2}^2. \tag{26}$$

By applying the same arguments again, we obtain

$$\left|I_3\right| \leq c\|\boldsymbol{F}\|_{\boldsymbol{L}^2(\Omega_b)}^2 + c\|\boldsymbol{u}^n - \boldsymbol{u}_d\|_{\boldsymbol{L}^2(\Omega_b)}^2 \tag{27}$$

and

$$\left|I_4\right| \leq \delta \|\boldsymbol{u}^n - \boldsymbol{u}_d\|_{\boldsymbol{L}^2(\Omega_b)}^2 + C(\delta) \|\partial_t \boldsymbol{u}_d\|_{\boldsymbol{H}^{-1}(\Omega_b)}^2. \tag{28}$$

Combining the results obtained in (25), (26), (27), and (28), and taking δ such that the constant $C\left(\underline{\nu}, \delta\right) = \dfrac{\underline{\nu}}{2} - \delta > 0$, we can derive

$$\begin{aligned} &\frac{d}{dt} \|\boldsymbol{u}^n - \boldsymbol{u}_d\|_{\boldsymbol{L}^2(\Omega_b)}^2 + C\left(\underline{\nu}, \delta\right) \|\boldsymbol{u}^n - \boldsymbol{u}_d\|_{\boldsymbol{H}^1(\Omega_b)}^2 \\ &\quad \leq C\|\boldsymbol{F}\|_{\boldsymbol{L}^2(\Omega_b)}^2 + C\|\partial_t \boldsymbol{u}_d\|_{\boldsymbol{H}^{-1}(\Omega_b)}^2 + C\left(\delta, \overline{\nu}\right) \|\nabla \boldsymbol{u}_d\|_{L^2}^2 + C\|\boldsymbol{u}^n - \boldsymbol{u}_d\|_{\boldsymbol{L}^2}^2 \left(1 + \|\nabla \boldsymbol{u}_d\|_{L^2}^{\frac{1}{1-\zeta}}\right). \end{aligned} \tag{29}$$

Since $\boldsymbol{u}_d \in \boldsymbol{L}^4\left(0, T; H^1(\Omega_b)\right)$, $\partial_t \boldsymbol{u}_d \in \boldsymbol{L}^2\left(0, T; \boldsymbol{H}^{-1}\left(\Omega_b\right)\right)$, $\boldsymbol{F} \in \boldsymbol{L}^2\left(\Omega_T\right)$, $\boldsymbol{u}^n(0)$ and $\boldsymbol{u}_d(0) \in L^2\left(\Omega_b, \mathbb{R}^3\right)$, integrating (29) over $(0, T)$ with $0 < t \leq T$, we can apply the Gröenwall inequality to obtain:

$$\sup_{0<t\leq T} \|\boldsymbol{u}^n(t) - \boldsymbol{u}_d(t)\|_{\boldsymbol{L}^2(\Omega_b, \mathbb{R}^3)}^2 \leq C, \tag{30}$$

where $C > 0$ is a constant depending on the L^2 norm of $\boldsymbol{u}_d$, $\partial_t \boldsymbol{u}_d$, $\boldsymbol{F}$, $\boldsymbol{u}_0$ and $\boldsymbol{u}_{d,0}$. Integrating again (29) in time leads to the following inequality:

$$\int_0^T \|\boldsymbol{u}^n(t)\|^2_{H^1(\Omega_b,\mathbb{R}^3)}\, dt \leq C. \tag{31}$$

Since the assumption (9), $\{\boldsymbol{u}^n\}_{n=1}^{\infty}$ is bounded in $L^{\infty}\left(0,T;\boldsymbol{L}^2\left(\Omega_b\right)\right) \cap L^2\left(0,T;\boldsymbol{H}^1\left(\Omega_b\right)\right)$ (cf. (30) and (31)) and $\boldsymbol{F}^n$ is bounded in $L^2\left(0,T;L^2\left(\Omega_b\right)\right)$, then we have that $\{\partial_t \boldsymbol{u}^n\}_{n=1}^{\infty}$ is bounded in $L^1\left(0,T;\left(\mathcal{H}_{\boldsymbol{0}}^{\boldsymbol{u}}\right)'\right)$. Indeed, for all $\boldsymbol{w} \in \mathcal{H}_{\boldsymbol{0}}^{\boldsymbol{u}}$ we have that

$$\begin{aligned}
|\langle \partial_t \boldsymbol{u}^n, \psi\rangle| &= |-a_{\boldsymbol{u}}\left(\theta_b^n;\boldsymbol{u}^n,\boldsymbol{\psi}\right) - b\left(\boldsymbol{u}^n,\boldsymbol{u}^n,\boldsymbol{\psi}\right) + \left(\boldsymbol{F}^n,\boldsymbol{\psi}\right)| \\
&\leq |a_{\boldsymbol{u}}\left(\theta_b^n;\boldsymbol{u}^n,\boldsymbol{\psi}\right)| + |b\left(\boldsymbol{u}^n,\boldsymbol{u}^n,\boldsymbol{\psi}\right)| + |\left(\boldsymbol{F}^n,\boldsymbol{\psi}\right)| \\
&\leq \bar{\nu}\|\nabla \boldsymbol{u}^n\|_{L^2}\|\nabla \boldsymbol{\psi}\|_{L^2} + c\|\boldsymbol{u}^n\|_{L^2}^{(1-\zeta)}\|\boldsymbol{u}^n\|_{H^1}^{\zeta+1}\|\boldsymbol{\psi}\|_{H^1} + \|\boldsymbol{F}^{\boldsymbol{n}}\|_{L^2}\|\boldsymbol{\psi}\|_{L^2}, \text{ where } \zeta = N/4 \\
&\leq C_1\|\nabla \boldsymbol{u}^n\|_{L^2}\|\boldsymbol{\psi}\|_{H^1} + C_2\|\boldsymbol{u}^n\|_{H^1}^2\|\boldsymbol{\psi}\|_{H^1} + C_3\|\boldsymbol{F}^{\boldsymbol{n}}\|_{L^2}\|\boldsymbol{\psi}\|_{H^1},
\end{aligned}$$

where c_1, c_2 and c_3 are positives constants. Further, (recall that $\boldsymbol{u}^n \in L^2\left(0,T;\boldsymbol{H}^1\left(\Omega_b\right)\right)$)

$$\begin{aligned}
\|\partial_t \boldsymbol{u}^n\|_{L^1\left(0,T;\left(\mathcal{H}_{\boldsymbol{0}}^{\boldsymbol{u}}\right)'\right)} &\leq C_1 T^{1/2}\left(\int_0^T \|\nabla \boldsymbol{u}^n\|_{L^2}^2\, dt\right)^{1/2} + C_2\int_0^T \|\boldsymbol{u}^n\|_{H^1}^2\, dt + C_3 T^{1/2}\left(\int_0^T \|\boldsymbol{F}\|_{L^2}^2\, dt\right)^{1/2} \\
&\leq C.
\end{aligned} \tag{32}$$

This achieves the estimate (21).

Proof of (22). By the maximum principle, we can deduce from the equation for φ_i^n the following inequality:

$$\underline{\varphi}_d \leq \varphi_b^n\left(t_1,x_1\right),\ \varphi_{ts}^n\left(t_2,x_2\right) \leq \overline{\varphi}_d \qquad \text{for all } \left(t_1,x_1\right) \in \Omega_{T,b},\ \left(t_2,x_2\right) \in \Omega_{T,ts}, \tag{33}$$

where $\underline{\varphi}_d = \min\limits_{(t,x)\in\overline{\Omega}_{T,b}\cup\overline{\Omega}_{T,ts}} \varphi_d(t,x)$ and $\overline{\varphi}_d = \max\limits_{(t,x)\in\overline{\Omega}_{T,b}\cup\overline{\Omega}_{T,ts}} \varphi_d(t,x)$. We define $\underline{\sigma} = \min\{\underline{\sigma}_b, \underline{\sigma}_{ts}\}$ and $\overline{\sigma} = \max\{\overline{\sigma}_b, \overline{\sigma}_{ts}\}$. Now, by substituting $\phi_i = \varphi_i^n - \varphi_d$ into (20), we can derive the following equation:

$$\begin{aligned}
\underline{\sigma}\sum_{i=b,ts}\iint_{\Omega_{T,i}} \left|\nabla\varphi_i^n\right|^2\, d\mathbf{x}\, dt &\leq \sum_{i=b,ts}\iint_{\Omega_{T,i}} \sigma_i\left(\theta_i^n\right)\nabla\varphi_i^n\cdot\nabla\varphi_i^n\, d\mathbf{x}\, dt \\
&= \sum_{i=b,ts}\iint_{\Omega_{T,i}} \sigma_i\left(\theta_i^n\right)\nabla\varphi_i^n\cdot\nabla\varphi_d\, d\mathbf{x}\, dt \\
&\leq \frac{\underline{\sigma}}{2}\sum_{i=b,ts}\iint_{\Omega_{T,i}} \left|\nabla\varphi_i^n\right|^2\, d\mathbf{x}\, dt + C\left(\underline{\sigma},\overline{\sigma}\right)\sum_{i=b,ts}\iint_{\Omega_{T,i}} \left|\nabla\varphi_d\right|^2\, d\mathbf{x}\, dt,
\end{aligned} \tag{34}$$

where we have used the assumptions (9) and the constant $C\left(\underline{\sigma},\overline{\sigma}\right) > 0$ is depending on $\underline{\sigma}$ and $\overline{\sigma}$. This leads to the following conclusion for $i = b, ts$:

$$\sum_{i=b,ts}\iint_{\Omega_{T,i}} \left|\nabla\varphi_i^n\right|^2\, d\mathbf{x}\, dt \leq C. \tag{35}$$

Proof of (23). Let us introduce $\underline{\eta} = \min\{\underline{\eta}_b, \underline{\eta}_{ts}\} > 0$ and $\overline{\eta} = \max\{\overline{\eta}_b, \overline{\eta}_{ts}\} > 0$. Now, we focus on (20) without considering the time integration. We use the test function $S_i = \theta_i^n(t) - \theta_d(t) \in \mathcal{H}_0^{\theta_i}$. This allows us to derive the following inequality:

$$
\begin{aligned}
&\frac{1}{2}\sum_{i=b,ts}\frac{d}{dt}\|\theta_i^n(t)-\theta_d(t)\|_{L^2}^2+\underline{\eta}\sum_{i=b,ts}\int_{\Omega_i}|\nabla\left(\theta_i^n(t)-\theta_d(t)\right)|^2\,d\mathbf{x}\\
&\quad\le\sum_{i=b,ts}\Big(\frac{1}{2}\frac{d}{dt}\|\theta_i^n(t)-\theta_d(t)\|_{L^2}^2+a_{\theta_i}\left(\theta_i^n,\theta_i^n-\theta_d(t),\theta_i^n(t)-\theta_d(t)\right)\Big)\\
&\quad=-d\left(\boldsymbol{u}^n(t),\theta_b^n(t),\theta_b^n(t)-\theta_d(t)\right)-\sum_{i=b,ts}a_{\theta_i}\left(\theta_i^n,\theta_d(t),\theta_i^n(t)-\theta_d(t)\right)+\sum_{i=b,ts}c_{\varphi_i}\left(\theta_i^n;\varphi_i^n,\theta_i^n(t)-\theta_d(t)\right)\\
&\qquad-\sum_{i=b,ts}\int_{\Omega_i}\partial_t\theta_d(t)\left(\theta_i^n(t)-\theta_d(t)\right)\,d\mathbf{x}\\
&\quad:=J_1+J_2+J_3+J_4.
\end{aligned}
\tag{36}
$$

We reformulate the first term in (36) as follows: (Recall that $\operatorname{div}\boldsymbol{u}^n=0$ and $\theta_b=\theta_s$ on Σ_8)

$$
\begin{aligned}
-J_1&=d\left(\boldsymbol{u}^n(t),\theta_b^n(t),\theta_b^n(t)-\theta_d(t)\right)\\
&=\int_{\Omega_b}\boldsymbol{u}^n\cdot\nabla\left(\theta_b^n-\theta_d(t)\right)\left(\theta_b^n(t)-\theta_d(t)\right)\,d\mathbf{x}+\int_{\Omega_b}\boldsymbol{u}^n\cdot\nabla\theta_d(t)\left(\theta_b^n(t)-\theta_d(t)\right)\,d\mathbf{x}\\
&=-\frac{1}{2}\int_{\Omega_b}\operatorname{div}\boldsymbol{u}^n\,\left(\theta_b^n-\theta_d(t)\right)^2\,d\mathbf{x}+\frac{1}{2}\int_{\Sigma_b}\boldsymbol{u}^n\cdot\boldsymbol{n}_b\,\left(\theta_b^n-\theta_d(t)\right)^2\,dy+\int_{\Omega_b}\boldsymbol{u}^n\cdot\nabla\theta_d(t)\left(\theta_b^n(t)-\theta_d(t)\right)\,d\mathbf{x}\\
&=\int_{\Omega_b}\boldsymbol{u}^n\cdot\nabla\theta_d(t)\left(\theta_b^n(t)-\theta_d(t)\right)\,d\mathbf{x}.
\end{aligned}
\tag{37}
$$

Now, to get the estimate of J_1, we applied the Sobolev embedding $H^1\hookrightarrow L^p$ with $1\le p\le 6$, used Hölder's inequality and Young's inequality with parameter δ; then, we obtained the following estimation:

$$
\begin{aligned}
\left|J_1\right|&=\left|-d\left(\boldsymbol{u}^n(t),\theta_d(t),\theta_b^n(t)-\theta_d(t)\right)\right|\\
&\le\|\boldsymbol{u}^n(t)\|_{\mathbf{L}^4}\left\|\theta_b^n(t)-\theta_d(t)\right\|_{\mathbf{L}^4}\left\|\nabla\theta_d(t)\right\|_{L^2}\\
&\le c\|\boldsymbol{u}^n(t)\|_{\mathbf{H}^1}\left\|\theta_b^n(t)-\theta_d(t)\right\|_{\mathbf{H}^1}\left\|\nabla\theta_d(t)\right\|_{L^2}\\
&\le\frac{\delta}{2}\left\|\theta_b^n(t)-\theta_d(t)\right\|_{H^1}^2+C(\delta)\|\boldsymbol{u}^n(t)\|_{\mathbf{H}^1}^2\left\|\nabla\theta_d(t)\right\|_{\mathbf{L}^2}^2.
\end{aligned}
\tag{38}
$$

From the definition of the form a_{θ_i}, we have

$$
\begin{aligned}
\left|a_{\theta_i}\left(\theta_i^n,\theta_d(t),\theta_i^n(t)-\theta_d(t)\right)\right|&=\left|\int_{\Omega_i}\eta_i\left(\theta_i^n\right)\nabla\theta_d(t)\nabla\left(\theta_i^n-\theta_d(t)\right)\,d\mathbf{x}\right|\\
&\le\overline{\eta}\|\nabla\theta_d(t)\|_{\mathbf{L}^2(\Omega_i)}\|\nabla\left(\theta_i^n(t)-\theta_d(t)\right)\|_{\mathbf{L}^2(\Omega_i)}\\
&\le\delta\|\theta_i^n(t)-\theta_d(t)\|_{H^1(\Omega_i)}^2+C\left(\delta\right)\|\nabla\theta_d(t)\|_{\mathbf{L}^2(\Omega_i)}^2,
\end{aligned}
$$

for $i=b,\,ts$ where $C(\delta)>0$. This implies that

$$
\left|J_2\right|\le\delta\sum_{i=b,ts}\|\theta_i^n(t)-\theta_d(t)\|_{H^1(\Omega_i)}^2+C\left(\delta\right)\sum_{i=b,ts}\|\nabla\theta_d(t)\|_{\mathbf{L}^2(\Omega_i)}^2.
\tag{39}
$$

According to the definition of c_{φ} and using Green's formula, we obtain the following expressions:

$$\begin{aligned}
J_3 &= \sum_{i=b,ts} c_{\varphi_i^n}\left(\theta_i^n;\varphi_i^n,\theta_i^n-\theta_d\right)\\
&= \sum_{i=b,ts}\int_{\Omega_i}\sigma_i\left(\theta_i^n\right)\nabla\varphi_i^n\cdot\nabla\varphi_i^n\left(\theta_i^n-\theta_d\right)\,d\mathbf{x}\\
&= \sum_{i=b,ts}\int_{\Omega_i}\sigma_i\left(\theta_i^n\right)\nabla\varphi_i^n\cdot\nabla\left(\varphi_i^n\left(\theta_i^n-\theta_d\right)\right)\,d\mathbf{x}-\sum_{i=b,ts}\int_{\Omega_i}\sigma_i\left(\theta_i^n\right)\varphi_i^n\nabla\varphi_i^n\cdot\nabla\left(\theta_i^n-\theta_d\right)\,d\mathbf{x}\\
&= \sum_{i=b,ts}\int_{\Sigma_i}\left(\sigma_i\left(\theta_i^n\right)\nabla\varphi_i^n\right)\cdot\boldsymbol{n}_i\varphi_i^n\left(\theta_i^n-\theta_d\right)\,dy-\sum_{i=b,ts}\int_{\Omega_i}\nabla\cdot\left(\sigma_i\left(\theta_i^n\right)\nabla\varphi_i^n\right)\varphi_i^n\left(\theta_i^n-\theta_d\right)\,d\mathbf{x}\\
&\qquad-\sum_{i=b,ts}\int_{\Omega_i}\sigma_i\left(\theta_i^n\right)\varphi_i^n\nabla\varphi_i^n\cdot\nabla\left(\theta_i^n-\theta_d\right)\,d\mathbf{x}\\
&= -\sum_{i=b,ts}\int_{\Omega_i}\sigma_i\left(\theta_i\right)\varphi_i^n\nabla\varphi_i^n\cdot\nabla\left(\theta_i^n-\theta_d\right)\,d\mathbf{x}.
\end{aligned}\tag{40}$$

Then, by (33) and (35), we conclude that:

$$\begin{aligned}
\left|J_3\right| &= \left|-\sum_{i=b,ts}\int_{\Omega_i}\sigma_i\left(\theta_i^n\right)\varphi_i^n\nabla\varphi_i^n\cdot\nabla\left(\theta_i^n-\theta_d\right)\,d\mathbf{x}\right|\\
&\leq\overline{\sigma}\sum_{i=b,ts}||\varphi_i^n||_{L^\infty}||\nabla\varphi_i^n||_{L^2}||\nabla\theta_i^n-\theta_d||_{L^2}\\
&\leq C\sum_{i=b,ts}||\nabla\varphi_i^n||_{\boldsymbol{L}^2}||\theta_i^n-\theta_d||_{H^1}\\
&\leq\delta\sum_{i=b,ts}||\theta_i^n-\theta_d||_{H^1}^2+C\left(\delta\right)\sum_{i=b,ts}||\nabla\varphi_i^n||_{\boldsymbol{L}^2}^2.
\end{aligned}\tag{41}$$

Similarly to J_3, we have for J_4

$$\left|J_4\right|\leq\delta\sum_{i=b,ts}||\theta_i^n-\theta_d||_{H^1}^2+C(\delta)\sum_{i=b,ts}\left\|\partial_t\theta_d(t)\right\|_{H^{-1}(\Omega_i)}^2.\tag{42}$$

Now, choosing δ sufficiently small, using the estimates (31), (35), (38), (39), (41) and (42) that leads to the following estimate

$$\begin{aligned}
&\frac{d}{dt}\left(\sum_{i=b,ts}\left\|\theta_i^n(t)-\theta_d(t)\right\|_{L^2(\Omega_i)}^2\right)+C_1\sum_{i=b,ts}||\theta_i^n(t)-\theta_d(t)||_{H^1}^2\\
&\qquad\leq C_2\left(\sum_{i=b,ts}\left\|\partial_t\theta_d(t)\right\|_{H^{-1}(\Omega_i)}^2+\sum_{i=b,ts}||\nabla\theta_d(t)||_{\boldsymbol{L}^2}^2+\sum_{i=b,ts}||\nabla\varphi_i^n||_{\boldsymbol{L}^2}^2+\left\|\boldsymbol{u}^n(t)\right\|_{\mathbf{H}^1}^2\left\|\nabla\theta_d(t)\right\|_{\mathbf{L}^2}^2\right)\\
&\qquad\quad+C_3\sum_{i=b,ts}\left\|\theta_i^n(t)-\theta_d(t)\right\|_{L^2(\Omega_i)}^2,
\end{aligned}\tag{43}$$

for some constants $C_1>0$, $C_2>0$ and $C_3>0$. Integrating (43) over $(0,T)$ with $0<t\leq T$, we get that

$$\sum_{i=b,ts}\left\|\theta_i^n(t)-\theta_d(t)\right\|_{L^2(\Omega_i)}^2\leq\sum_{i=b,ts}\left\|\theta_i^n(0)-\theta_d(0)\right\|_{L^2}^2+\alpha(t)+C_3\int_0^t\sum_{i=b,ts}\left\|\theta_i^n(s)-\theta_d(s)\right\|_{L^2(\Omega_i)}^2ds,\tag{44}$$

where

$$\alpha(t)=C_2\int_0^t\left(\sum_{i=b,ts}\left\|\partial_t\theta_d(s)\right\|_{H^{-1}(\Omega_i)}^2+\sum_{i=b,ts}||\nabla\theta_d(s)||_{\boldsymbol{L}^2}^2+\sum_{i=b,ts}||\nabla\varphi_i^n(s)||_{\boldsymbol{L}^2}^2+\left\|\boldsymbol{u}^n(s)\right\|_{\mathbf{H}^1}^2\left\|\nabla\theta_d(s)\right\|_{\mathbf{L}^2}^2\right)ds>0.$$

The Gronwall's inequality implies

$$\sum_{i=b,ts} \sup_{0<t\leq T} \left\|\theta_i^n(t) - \theta_d\right\|^2_{L^2(\Omega_i)} \leq C, \tag{45}$$

for some constant $C > 0$. By the estimates (43) and (45), we can conclude that there exist constants $C_1 > 0$ and $C_2 > 0$ such that

$$\sum_{i=b,ts} \left\|\theta_i^n(t)\right\|_{L^\infty(0,T;L^2(\Omega_i))} \leq C_1, \tag{46}$$

$$\sum_{i=b,ts} \left\|\theta_i^n(t)\right\|_{L^2(0,T;H^1(\Omega_i))} \leq C_2. \tag{47}$$

Now, since the assumption (9) be satisfied and from (46) and (47), we deduce that $\left\{\theta_i^n\right\}_{n=1}^{\infty}$ is bounded in $L^\infty\left(0,T;L^2\left(\Omega_i\right)\right) \cap L^2\left(0,T;H^1\left(\Omega_i\right)\right)$, for all $i = b, ts$. Thus, we collect the previous results on $\boldsymbol{u}^n$ and φ_i^n to obtain that $a_{\theta_i}\left(\theta_i^n;\theta_i^n,\cdot\right)$, $d\left(\boldsymbol{u}^n,\theta_b^n,\cdot\right)$ and $c_{\varphi_i}\left(\theta_i^n,\varphi_i^n,\cdot\right)$ are bounded in $L^2\left(0,T;H^{-1}\left(\Omega_i\right)\right)$, $L^1\left(0,T;H^{-1}\left(\Omega_b\right)\right)$ and $L^2\left(0,T;H^{-1}\left(\Omega_i\right)\right)$, respectively. Consequently, $\left\{\partial_t\theta_i^n\right\}_{n=1}^{\infty}$ is bounded in $L^1\left(0,T;H^{-1}\left(\Omega_i\right)\right)$ for all $i = b, ts$. Indeed

$$\begin{aligned}
\sum_{i=b,ts}\int_0^T \|\partial_t\theta_i^n\|_{H^{-1}(\Omega_i)}\,dt \leq{}& \sum_{i=b,ts}\int_0^T \|a_{\theta_i}\left(\theta_i^n;\theta_i^n,\cdot\right)\|_{H^{-1}(\Omega_i)}\,dt + \int_0^T \|d\left(\boldsymbol{u}^n,\theta_b^n,\cdot\right)\|_{H^{-1}(\Omega_b)}\,dt \\
&+ \sum_{i=b,ts}\int_0^T \|c_{\varphi_i}\left(\theta_i^n,\varphi_i^n,\cdot\right)\|_{H^{-1}(\Omega_i)}\,dt \\
\leq{}& C\left(\overline{\eta},T\right)\sum_{i=b,ts}\|\nabla\theta_i^n\|_{L^2(0,T;L^2)} + c_1\|\boldsymbol{u}^n\|_{L^2(0,T;H^1(\Omega_b))}\|\nabla\theta_b^n\|_{L^2(0,T;L^2(\Omega_b))} \\
&+ C\left(\overline{\sigma},T\right)\sum_{i=b,ts}\|\varphi_i^n\|_{L^\infty(0,T;L^\infty(\Omega_i))}\|\nabla\varphi_i^n\|_{L^2(0,T;L^2(\Omega_i))} \\
\leq{}& C,
\end{aligned}$$

for some constant $C > 0$.

■

3.3. Passage to the limit and concluding the proof of Theorem 2.1

Thanks to Lemma 3.1, there exist subsequences of $\{\boldsymbol{u}^n\}_{n=1}^{\infty}$, $\left\{\varphi_i^n\right\}_{n=1}^{\infty}$, and $\left\{\theta_i^n\right\}_{n=1}^{\infty}$, which will be still denoted (for simplicity) as $\{\boldsymbol{u}^n\}_{n=1}^{\infty}$, $\left\{\varphi_i^n\right\}_{n=1}^{\infty}$, and $\left\{\theta_i^n\right\}_{n=1}^{\infty}$(for $i = b,\ ts$), respectively, such that:

$$\begin{cases}
\boldsymbol{u}^n \rightharpoonup \boldsymbol{u} \text{ weakly in } L^2\left(0,T;\mathcal{H}_{\mathbf{0}}^{\boldsymbol{u}}\right), \\
\partial_t\boldsymbol{u}^n \rightharpoonup \partial_t\boldsymbol{u} \text{ weakly in } L^1\left(0,T;\left(\mathcal{H}_{\mathbf{0}}^{\boldsymbol{u}}\right)'\right), \\
\nabla\boldsymbol{u}^n \rightharpoonup \nabla\boldsymbol{u} \text{ weakly in } L^2\left(0,T;\boldsymbol{L}^2\right),
\end{cases} \tag{48}$$

$$\begin{cases}
\varphi_i^n \rightharpoonup \varphi_i \text{ weakly in } L^\infty\left(0,T;L^\infty\left(\Omega_i\right)\right), \\
\varphi_i^n \rightharpoonup \varphi_i \text{ weakly in } L^2\left(0,T;H^1\left(\Omega_i\right)\right), \\
\varphi_i^n \to \varphi_i \text{ strongly in } L^2\left(0,T;L^2\left(\Omega_i\right)\right), \\
\nabla\varphi_i^n \rightharpoonup \nabla\varphi_i \text{ weakly in } L^2\left(I;\boldsymbol{L}^2\left(\Omega_i\right)\right),
\end{cases} \tag{49}$$

$$\begin{cases}
\theta_i^n \rightharpoonup \theta_i \text{ weakly in } L^2\left(0,T;H^1\right), \\
\partial_t\theta_i^n \rightharpoonup \partial_t\theta_i \text{ weakly in } L^1\left(0,T;H^{-1}\right), \\
\nabla\theta_i^n \rightharpoonup \nabla\theta_i \text{ weakly in } L^2\left(0,T;\mathbf{L}^2\right).
\end{cases} \tag{50}$$

By the Aubin–Lions–Simon compactness theorem ($\left\{u \in L^2\left(0,T,H^1\right), \partial_t u \in L^1\left(0,T,H^{-1}\right)\right\} \hookrightarrow\hookrightarrow L^2\left(0,T,L^2\right)$, see also [16, Theorem II.5.16]), we get for $i = b, ts$:

$$\begin{cases} \boldsymbol{u}^n \to \boldsymbol{u} \text{ strongly in } L^2\left(0,T;\mathbf{L}^2\right), \\ \boldsymbol{u}^n \to \boldsymbol{u} \text{ almost everywhere in } \Omega_{b,T}, \\ \theta_i^n \to \theta_i \text{ strongly in } L^2\left(0,T;L^2\right), \\ \theta_i^n \to \theta_i \text{ almost everywhere in } \Omega_T. \end{cases} \tag{51}$$

Next, denote the differences $\tilde{\theta}_i^n = \theta_i^n - \theta_i$, $\tilde{\boldsymbol{u}}^n = \boldsymbol{u}^n - \boldsymbol{u}$, and $\tilde{\varphi}_i^n = \varphi_i^n - \varphi_i$ for $i = b, ts$. Then, by choosing the test functions $\left(\boldsymbol{\psi}, S_i, \phi_i\right) \in \mathcal{H}_{\mathbf{0}}^{\boldsymbol{u}} \times \mathcal{H}_0^{\theta_i} \times \mathcal{H}_0^{\varphi_i}$ in the weak formulation (20) and using the results (48)-(51), as well as the continuity of ν, η_i, and σ_i, we obtain the following limits:

$$\begin{aligned} a_{\boldsymbol{u}}\left(\theta_b^n;\boldsymbol{u}^n,\boldsymbol{\psi}\right) - a_{\boldsymbol{u}}\left(\theta_b;\boldsymbol{u},\boldsymbol{\psi}\right) &= a_{\boldsymbol{u}}\left(\theta_b^n;\tilde{\boldsymbol{u}}^n,\boldsymbol{\psi}\right) + \int_{\Omega_b}\left[\nu\left(\theta_b^n\right) - \nu\left(\theta_b\right)\right]\mathbb{D}(\boldsymbol{u}) : \nabla\boldsymbol{\psi}\, d\mathbf{x} \\ &\leq \bar{\nu}\int_{\Omega_b}\mathbb{D}\left(\tilde{\boldsymbol{u}}^{\boldsymbol{n}}\right) : \nabla\boldsymbol{\psi}\, d\mathbf{x} + \int_{\Omega_b}\left[\nu\left(\theta_b^n\right) - \nu\left(\theta_b\right)\right]\mathbb{D}(\boldsymbol{u}) : \nabla\boldsymbol{\psi}\, d\mathbf{x}. \end{aligned} \tag{52}$$

Based on the weak convergence of $\nabla\boldsymbol{u}^n$ to $\nabla\boldsymbol{u}$ in $\boldsymbol{L}^2\left(\Omega_b\right)$, the first integral goes to 0 when n goes to ∞. Furthermore, we infer the second quantity's convergence to 0 using the Lebesgue-dominated convergence (see, for example, [11]). Then, we get

$$a_{\boldsymbol{u}}\left(\theta_b^n;\boldsymbol{u}^n,\boldsymbol{\psi}\right) \xrightarrow{n\longrightarrow\infty} a_{\boldsymbol{u}}\left(\theta_b;\boldsymbol{u},\boldsymbol{\psi}\right). \tag{53}$$

Furthermore, following the sames methods that proved (53), we also show that :

$$\begin{aligned} a_\varphi\left(\theta_i^n,\varphi_i^n,\phi_i\right) - a_\varphi\left(\theta_i,\varphi_i,\phi_i\right) &= a_\varphi\left(\theta_i,\tilde{\varphi}_i^n,\phi_i\right) + \int_{\Omega_i}\left[\sigma_i\left(\theta_i^n\right) - \sigma_i\left(\theta_i\right)\right]\nabla\varphi_i\cdot\nabla\phi_i\, d\mathbf{x} \xrightarrow{n\longrightarrow\infty} 0, \\ a_\theta\left(\theta_i^n,\theta_i^n,S_i\right) - a_\theta\left(\theta_i;\theta_i,S_i\right) &= a_\theta\left(\theta_i^n,\tilde{\theta}_i^n,S_i\right) + \int_{\Omega_i}\left[\eta_i\left(\theta_i^n\right) - \eta_i\left(\theta_i\right)\right]\nabla\theta_i\cdot\nabla S_i\, d\mathbf{x} \xrightarrow{n\longrightarrow\infty} 0. \end{aligned} \tag{54}$$

From the compact embedding $\boldsymbol{H}^1\left(\Omega_b\right) \hookrightarrow\hookrightarrow \boldsymbol{L}^q\left(\Omega_b\right)$ (resp. $H^1\left(\Omega_i\right) \hookrightarrow\hookrightarrow L^q(\Omega_i)$, for $i = b, ts$), with $1 \leq q \leq 6$(for $N = 3$). Then, using again Lebesgue-dominated convergence, we have the followings strong convergences:

$$b\left(\boldsymbol{u}^n,\boldsymbol{u}^n,\boldsymbol{\psi}\right) \xrightarrow{n\longrightarrow\infty} b\left(\boldsymbol{u},\boldsymbol{u},\boldsymbol{\psi}\right), \tag{55}$$

$$d\left(\boldsymbol{u}^n,\theta_b^n,S_b\right) \xrightarrow{n\longrightarrow\infty} d\left(\boldsymbol{u},\theta_b,S_b\right). \tag{56}$$

Finally, using the results of (49) and continuity of σ_i, we obtain

$$\begin{aligned} c_\varphi\left(\theta_i^n,\varphi_i^n,S_i\right) - c_\varphi\left(\theta_i,\varphi_i,S_i\right) &= \int_{\Omega_i}\sigma_i\left(\theta_i^n\right)\varphi_i^n\cdot\nabla\varphi_i^n\cdot\nabla S_i\, d\mathbf{x} - \int_{\Omega}\sigma_i\left(\theta_i\right)\varphi_i\cdot\nabla\varphi_i\nabla S_i\, d\mathbf{x} \\ &= \left(\int_{\Omega_i}\sigma_i\left(\theta_i^n\right)\tilde{\varphi}_i^n\cdot\nabla\varphi_i^n\cdot\nabla S_i\, d\mathbf{x} + \int_{\Omega}\left[\sigma_i\left(\theta_i^n\right) - \sigma_i\sigma_i\left(\theta_i\right)\right]\varphi_i\nabla\varphi_i^n\cdot\nabla S_i\, d\mathbf{x}\right. \\ &\qquad \left. + \int_{\Omega_i}\sigma_i(\theta_i)\tilde{\varphi}_i^n\cdot\nabla\varphi_i^n\cdot\nabla S_i\, d\mathbf{x}\right) \xrightarrow{n\longrightarrow\infty} 0. \end{aligned} \tag{57}$$

Now, by exploiting the results (53)-(57) we can pass immediately to the limit in the weak approximate formulation (15) as $n \longrightarrow \infty$. The result is: the triple $(\boldsymbol{u}, \theta_i, \varphi_i)$ satisfies the following variational formulation:

$$\begin{aligned} &\langle\partial_t\boldsymbol{u},\boldsymbol{\psi}\rangle + a_{\boldsymbol{u}}\left(\theta_b;\boldsymbol{u},\boldsymbol{\psi}\right) + b\left(\boldsymbol{u},\boldsymbol{u},\boldsymbol{\psi}\right) - (\boldsymbol{F},\boldsymbol{\psi}) = 0, \\ &\sum_{i=b,ts}\left(\langle\partial_t\theta_i,S_i\rangle + a_{\theta_i}\left(\theta_i;\theta_i,S_i\right) - c_{\varphi_i}\left(\theta_i,\varphi_i,S_i\right)\right) + d\left(\boldsymbol{u},\theta_b,S_b\right) = 0, \\ &\sum_{i=b,ts} a_{\varphi_i}\left(\theta_i;\varphi_i,\phi_i\right) = 0, \end{aligned} \tag{58}$$

for every $(\boldsymbol{\psi}, S_i, \phi_i) \in \mathcal{H}_{\mathbf{0}}^{\boldsymbol{u}} \times \mathcal{H}_0^{\theta_i} \times \mathcal{H}_0^{\varphi_i}$ with $S_b = S_{ts}$ on Σ_b^N and almost every $t \in I$ and the initial condition

$$\boldsymbol{u}(\boldsymbol{x}, 0) = \boldsymbol{u}_0(\boldsymbol{x}), \tag{59}$$

$$\theta_i(\boldsymbol{x}, 0) = \theta_i^0(\boldsymbol{x}), \quad \text{in } \Omega, \text{ for all } i = b, ts. \tag{60}$$

To complete the proof of Theorem 2.1, we also need to demonstrate that $\partial_t \boldsymbol{u} \in \mathrm{L}^1\left(0, T; (\mathcal{H}_0^{\boldsymbol{u}})'\right)$ and $\partial_t \theta_i \in L^1\left(0, T; \left(\mathcal{H}^{\theta_i}\right)'\right)$ for all $i = b, ts$. Indeed, the first equation of (58) can be expressed as follows:

$$\frac{\mathrm{d}}{\mathrm{d}t}\langle \boldsymbol{u}, \boldsymbol{\psi}\rangle = \langle \operatorname{div}\left(\nu\left(\theta_b\right)\mathbb{D}(\boldsymbol{u})\right) - \boldsymbol{B}(\boldsymbol{u}) + \boldsymbol{F}, \boldsymbol{\psi}\rangle \text{ for all } \boldsymbol{\psi} \in \mathcal{H}_0^{\boldsymbol{u}}. \tag{61}$$

On one hand, ν is bounded, the operator $-\operatorname{div}\left(\nu\left(\theta_b\right)\mathbb{D}(\boldsymbol{u})\right) : \mathcal{H}_0^{\boldsymbol{u}} \to (\mathcal{H}_0^{\boldsymbol{u}})'$ is linear and continuous, and $\boldsymbol{u} \in \mathrm{L}^2\left(0, T; \mathcal{H}_0^{\boldsymbol{u}}\right)$; this implies that $-\operatorname{div}\left(\nu\left(\theta_b\right)\mathbb{D}(\boldsymbol{u})\right) \in \mathrm{L}^2\left(0, T; \left(\mathcal{H}_0^{\boldsymbol{u}}\right)'\right)$. On the other hand, $\boldsymbol{F} \in \mathrm{L}^2\left(0, T; \boldsymbol{L}^2\left(\Omega_b\right)\right)$. By Lemma 2.1, we have established that $b(\boldsymbol{u}, \boldsymbol{u}, \boldsymbol{\psi}) = \langle \boldsymbol{B}(\boldsymbol{u}), \boldsymbol{\psi}\rangle$ is trilinear and continuous on $\mathcal{H}_0^{\boldsymbol{u}}$, and $\|\boldsymbol{B}(\boldsymbol{u})\|_{(\mathcal{H}_0^{\boldsymbol{u}})'} \leq \|\boldsymbol{u}\|^2_{\mathcal{H}_0^{\boldsymbol{u}}}$. Thus, $\boldsymbol{B}(\boldsymbol{u}) \in \mathrm{L}^1\left(0, T, (\mathcal{H}_0^{\boldsymbol{u}})'\right)$. Consequently, $\partial_t \boldsymbol{u} \in \mathrm{L}^1\left(0, T; \left(\mathcal{H}_0^{\boldsymbol{u}}\right)'\right)$.
In similar ways, the second equation of (58) can also be expressed by:

$$\sum_{i=b,ts} \langle \partial_t \theta_i, S_i\rangle = -\sum_{i=b,ts} a_{\theta_i}\left(\theta_i; \theta_i, S_i\right) - d\left(\boldsymbol{u}, \theta_b, S_b\right) + \sum_{i=b,ts} c_{\varphi_i}\left(\theta_i, \varphi_i, S_i\right) \text{ for all } S_i \in \mathcal{H}_0^{\theta_i}. \tag{62}$$

Since Assumption (9) is satisfied and $\theta_i \in L^2\left(0, T; \mathcal{H}_0^{\theta_i}\right)$, we deduce that $a_{\theta_i}\left(\theta_i; \theta_i, \cdot\right) \in L^2\left(0, T; L^2\left(\Omega_i\right)\right)$. Furthermore, we collect the result that $\boldsymbol{u} \in \mathrm{L}^2\left(0, T; \mathcal{H}_0^{\boldsymbol{u}}\right)$ and $\varphi_i \in L^2\left(0, T; \mathcal{H}_0^{\varphi_i}\right) \cap L^\infty\left(0, T; L^\infty\left(\Omega_i\right)\right)$ to get $d\left(\boldsymbol{u}, \theta_b, \cdot\right)$ and $c_{\varphi_i}\left(\theta_i, \varphi_i, \cdot\right)$ are bounded in $L^1\left(0, T; H^{-1}\left(\Omega_b\right)\right)$ and $L^2\left(0, T; H^{-1}\left(\Omega_i\right)\right)$, respectively. Consequently, $\partial_t \theta_i$ is bounded in $L^1\left(0, T; \left(\mathcal{H}^{\theta_i}\right)'\right)$ for $i = b,\ ts$.

Finally, to introduce the pressure π, we set

$$V(t) = \int_0^t \left(\nu\left(\theta_b\right)\mathbb{D}(\boldsymbol{u})\right)(s)\, ds,\ R(t) = \int_0^t (\boldsymbol{u}\cdot\nabla)\boldsymbol{u}(s)\, ds,\ \text{and}\ K(t) = \int_0^t \boldsymbol{F}(s)\, ds.$$

It is clear that $V, K, R \in C\left(0, T; \left(\mathrm{H}^1(\Omega)\right)'\right)$. Integrating (61) over $[0, t]$ yields

$$\langle \boldsymbol{u}(t) - \boldsymbol{u}_0 - \operatorname{div} V(t) + R(t) + K(t), \boldsymbol{\psi}\rangle = \mathbf{0} \text{ for all } t \in [0, T] \text{ and for all } \boldsymbol{\psi} \in \mathcal{H}_0^{\boldsymbol{u}}.$$

By application of the Rham theorem [33], we find, for each $t \in [0, T]$, the existence of some function $P(t) \in \mathrm{L}_0^2\left(\Omega_b\right)$ such that

$$\boldsymbol{u}(t) - \boldsymbol{u}_0 - \operatorname{div} V(t) + R(t) + K(t) + \nabla P = \mathbf{0},$$

where $\mathrm{L}_0^2(\Omega) = \left\{w \in \mathrm{L}^2\left(\Omega_b\right), \int_\Omega w\, \mathrm{d}\boldsymbol{x} = 0\right\}$. Therefore, $\nabla P \in C\left(0, T; \mathrm{H}^{-1}\left(\Omega_b\right)\right)$, and thus $P \in C\left(0, T; \mathrm{L}_0^2\left(\Omega_b\right)\right)$. By derivation with respect to t in the sense of distributions, we obtain

$$\partial_t \boldsymbol{u} - \operatorname{div}\left(\nu\left(\theta_b\right)\mathbb{D}(\boldsymbol{u})\right) + (\boldsymbol{u}\cdot\nabla)\boldsymbol{u} + \boldsymbol{F} + \nabla\pi = \mathbf{0},$$

where $\pi = \partial_t P \in W^{-1,\infty}\left(0, T; L_0^2\left(\Omega_b\right)\right)$.

4. Numerical approach

In this section we present the numerical procedure to solve the electro–thermo–fluid model (5). In this regard, the brief overview of the numerical discretization of finite element method approximation of aforesaid model is given. Next, we prove the existence of a discrete solution to the discrete problem. In addition, we indicate the main steps of the convergence proof of the finite element solution generated by the discrete problem. Subsequently, numerical results are provided to illustrate the influence of the presence of potential electrical in cardiac tissue, the saline viscosity and the external forces.

4.1. Existence of the numerical scheme

Let now give the discretization of our model. For this, let $\mathcal{T}_i$ be a regular partition of Ω_i into tetrahedra K_i with boundary ∂K_i and diameter h_{K_i} where $i = b, ts$. We define the mesh parameter $h = \max_{K_i \in \mathcal{T}_i}\{h_{K_i}\}$ and the associated finite element spaces $\boldsymbol{W}^h$ and V_i^h for the approximation of viscosity and, heats and electrical potentials, respectively (we use piecewise linear finite elements for heats and potentials). The involved spaces is defined as

$$\begin{aligned}
\boldsymbol{W}^h &= \{\boldsymbol{v} \in C^0(\bar{\Omega}_b) : \boldsymbol{v}|_{K_b} \in \mathbb{P}_2(K_b) \text{ for all } K_b \in \mathcal{T}_b\},\\
V_i^h &= \{S \in C^0(\bar{\Omega}_i) : S|_{K_i} \in \mathbb{P}_1(K_i) \text{ for all } K_i \in \mathcal{T}_i\}, \qquad \text{for } i = b, ts.
\end{aligned}$$

where $\mathbb{P}_k$, denotes the k-th degree piecewise polynomial space, with $k = 1, 2$. The semidiscrete Galerkin finite element formulation reads as follows for the electro-thermo-fluid RFA model equations (5). For $t > 0$, find $\boldsymbol{u}^h \in \boldsymbol{W}^h$, $\theta_i^h(t), \varphi_i^h(t) \in V_i^h$ and $\pi^h(t) \in V_b^h$ such that (with the standard finite element notation for L^2 scalar products) one has

$$\begin{aligned}
&\frac{d}{dt}\left(\boldsymbol{u}^h, \boldsymbol{\psi}^h\right)_{\Omega_b} + a_{\boldsymbol{u}}\left(\theta_b^h; \boldsymbol{u}^h, \boldsymbol{\psi}^h\right) + b\left(\boldsymbol{u}^h, \boldsymbol{u}^h, \boldsymbol{\psi}^h\right) - \left(\boldsymbol{F}^h, \boldsymbol{\psi}^h\right)_{\Omega_b} = 0,\\
&\sum_{i=b,ts} \frac{d}{dt}\left(\theta_i^h, S_i^h\right)_{\Omega_i} + \sum_{i=b,ts} a_{\theta_i}\left(\theta_i^h; \theta_i^h, S_i^h\right) + d\left(\boldsymbol{u}^h, \theta_b^h, S_b^h\right) - \sum_{i=b,ts} c_{\varphi_i}\left(\theta_i^h, \varphi_i^h, S_i^h\right) = 0,\\
&\sum_{i=b,ts} a_{\varphi_i}\left(\theta_i^h; \varphi_i^h, \phi_i^h\right) = 0,
\end{aligned} \tag{63}$$

for all test functions $\boldsymbol{\psi}^h \in \boldsymbol{W}^h$, $S_i^h \in V_i^h$ and $\phi_i^h \in V_i^h$, for $i = b, ts$, with $S_b^h = S_{ts}^h$ on $\Sigma_{T,7} \cup \Sigma_{T,8}$ and $\phi_b^h = \phi_{ts}^h$ on $\Sigma_{T,7} \cup \Sigma_{T,8}$. We define a time subdivision $t_0 = 0 < \cdots < t_M = T$, where M is an integer and the time steps is as follows $\Delta t := \frac{T}{M} = t_{n+1} - t_n$, $n = 0, \cdots, M-1$. This results in the following fully discrete method: for $t > 0$, find $\boldsymbol{u}^h \in \boldsymbol{W}^h$, $\theta_i^h(t), \varphi_i^h(t) \in V_i^h$ and $\pi^h(t) \in V_b^h$ such that

$$\begin{aligned}
\boldsymbol{u}^h(t,x) &= \sum_{n=1}^{M} \boldsymbol{u}^{h,n}(x) \mathbb{1}_{[(n-1)\Delta t, n\Delta t]}(t),\\
\theta_i^h(t,x) &= \sum_{n=1}^{M} \theta_i^{h,n}(x) \mathbb{1}_{[(n-1)\Delta t, n\Delta t]}(t),\\
\varphi_i^h(t,x) &= \sum_{n=1}^{M} \varphi_i^{h,n}(x) \mathbb{1}_{[(n-1)\Delta t, n\Delta t]}(t),
\end{aligned}$$

satisfy the following system

$$\begin{aligned}
&\left(\frac{\boldsymbol{u}^{h,n} - \boldsymbol{u}^{h,n-1}}{\Delta t}, \boldsymbol{\psi}^h\right)_{\Omega_b} + a_{\boldsymbol{u}}\left(\theta_b^{h,n-1}; \boldsymbol{u}^{h,n}, \boldsymbol{\psi}^h\right) + b\left(\boldsymbol{u}^{h,n}, \boldsymbol{u}^{h,n-1}, \boldsymbol{\psi}^h\right) - \left(\boldsymbol{F}^{h,n}, \boldsymbol{\psi}^h\right)_{\Omega_b} = 0,\\
&\sum_{i=b,ts}\left(\frac{\theta_i^{h,n} - \theta_i^{h,n-1}}{\Delta t}, S_i^h\right)_{\Omega_i} + \sum_{i=b,ts} a_{\theta_i}\left(\theta_i^{h,n-1}; \theta_i^{h,n}, S_i^h\right) + d\left(\boldsymbol{u}^{h,n}, \theta_b^{h,n}, S_b^h\right) - \sum_{i=b,ts} c_{\varphi_i}\left(\theta_i^{h,n}, \varphi_i^{h,n-1}, S_i^h\right) = 0,\\
&\sum_{i=b,ts} a_{\varphi_i}\left(\theta_i^{h,n-1}; \varphi_i^{h,n}, \phi_i^h\right) = 0,
\end{aligned} \tag{64}$$

for all test functions $\boldsymbol{\psi}^h \in \boldsymbol{W}^h$, $S_i^h \in V_i^h$ and $\phi_i^h \in V_i^h$, for $i = b, ts$, with $S_b^h = S_{ts}^h$ on $\Sigma_{T,7} \cup \Sigma_{T,8}$ and $\phi_b^h = \phi_{ts}^h$ on $\Sigma_{T,7} \cup \Sigma_{T,8}$ and for all $n \in \{1, \ldots, M\}$; the initials conditions takes the form (the initial conditions are projected on $\boldsymbol{W}^h$ and V_i^h by means of the L^2-Hilbertian projection $P_{\boldsymbol{W}^h}$ and $P_{V_i^h}$, respectively)

$$(\boldsymbol{u}^{h,0}, \theta_i^{h,0}) = (P_{\boldsymbol{W}^h}(\boldsymbol{u}_0), P_{V_i^h}(\theta_{i,0})).$$

The existence result for the finite element scheme is given by the following lemma.

Lemma 4.1. *Assume that (9), (10) and (11) hold. Then the problem (64) admits a discrete solution* $\left(\boldsymbol{u}^h, \theta_b^h, \theta_{ts}^h, \varphi_b^h, \varphi_{ts}^h\right)$.

Proof. Let $E_h := \boldsymbol{W}^h \times V_b^h \times V_{ts}^h \times V_b^h \times V_{ts}^h$ be a Hilbert space endowed with the obvious norm, let $Y^h := \left(\boldsymbol{u}^h, \theta_b^h, \theta_{ts}^h, \varphi_b^h, \varphi_{ts}^h\right)$ and $\Phi^h := \left(\boldsymbol{\psi}^h, S_b^h, S_{ts}^h, \phi_b^h, \phi_{ts}^h\right) \in E_h$ with $S_b^h = S_{ts}^h$ on $\Sigma_{T,7} \cup \Sigma_{T,8}$ and $\phi_b^h = \phi_{ts}^h$ on $\Sigma_{T,7} \cup \Sigma_{T,8}$. We now define the mapping $\mathcal{A} : E_h \to E_h$ by

$$\begin{aligned}\left[\mathcal{A}\left(Y^{h,n}\right), \Phi^h\right] = &\left(\frac{\boldsymbol{u}^{h,n} - \boldsymbol{u}^{h,n-1}}{\Delta t}, \boldsymbol{\psi}^h\right)_{\Omega_b} + a_{\boldsymbol{u}}\left(\theta_b^{h,n-1}; \boldsymbol{u}^{h,n}, \boldsymbol{\psi}^h\right) + b\left(\boldsymbol{u}^{h,n}, \boldsymbol{u}^{h,n-1}, \boldsymbol{\psi}^h\right) - \left(\boldsymbol{F}^{h,n}, \boldsymbol{\psi}^h\right)_{\Omega_b} \\ &+ \sum_{i=b,ts}\left(\frac{\theta_i^{h,n} - \theta_i^{h,n-1}}{\Delta t}, S_i^h\right)_{\Omega_i} + \sum_{i=b,ts} a_{\theta_i}\left(\theta_i^{h,n-1}; \theta_i^{h,n}, S_i^h\right) + d\left(\boldsymbol{u}^{h,n}, \theta_b^{h,n}, S_b^h\right) \\ &- \sum_{i=b,ts} c_{\varphi_i}\left(\theta_i^{h,n}, \varphi_i^{h,n-1}, S_i^h\right) + \sum_{i=b,ts} a_{\varphi_i}\left(\theta_i^{h,n-1}; \varphi_i^{h,n}, \phi_i^h\right),\end{aligned}$$

for all $\Phi^h \in E_h$. We have the following estimate from the same estimates as in subsection 3.2.

$$\left[\mathcal{A}\left(Y^{h,n}\right), \Phi^h\right] \le C \left\|Y^h\right\|_{E_h} \left\|\Phi^h\right\|_{E_h}, \quad \text{for all} \quad Y^h \text{ and } \Phi^h \text{ in } E_h.$$

This implies that $\mathcal{A}$ is continuous. The aim now is to show that

$$[\mathcal{A}(Y^{h,n}), Y^{h,n}] > 0 \quad \text{for} \left\|Y^{h,n}\right\|_{E_h} = r > 0, \tag{65}$$

for a sufficiently large r. We mention that from the trace embedding theorem, Young and Poincare inequalities,

$$\begin{aligned}\left[\mathcal{A}\left(Y^{h,n}\right), Y^{h,n}\right] \ge &\frac{1}{\Delta t}\left\|\boldsymbol{u}^{h,n}\right\|_{L^2}^2 - \frac{1}{\Delta t}\left(\boldsymbol{u}^{h,n-1}, \boldsymbol{u}^{h,n}\right)_{\Omega_b} + \underline{\nu}\left\|\boldsymbol{u}^{h,n}\right\|_{H^1}^2 - \left(\boldsymbol{F}^{h,n}, \boldsymbol{u}^{h,n}\right)_{\Omega_b} \\ &+ \frac{1}{\Delta t}\sum_{i=b,ts}\left\|\theta_i^{h,n}\right\|_{L^2}^2 - \frac{1}{\Delta t}\sum_{i=b,ts}\left(\theta_i^{h,n-1}, \theta_i^{h,n}\right)_{\Omega_i} + \sum_{i=b,ts}\underline{\eta}_i\left\|\theta_i^{h,n}\right\|_{H^1}^2 \\ &- \sum_{i=b,ts} c_{\varphi_i}\left(\theta_i^{h,n}, \varphi_i^{h,n-1}, \theta_i^{h,n}\right) + \sum_{i=b,ts}\underline{\sigma}_i\left\|\varphi_i^{h,n}\right\|_{H^1}^2, \\ \ge &\frac{1}{2\Delta t}\left\|\boldsymbol{u}^{h,n}\right\|_{L^2}^2 - \frac{1}{4\Delta t}\left\|\boldsymbol{u}^{h,n-1}\right\|_{L^2}^2 + \underline{\nu}\left\|\boldsymbol{u}^{h,n}\right\|_{H^1}^2 - C(\Delta t)\left\|\boldsymbol{F}^{h,n}\right\|_{L^2}^2 \\ &+ \frac{1}{2\Delta t}\sum_{i=b,ts}\left\|\theta_i^{h,n}\right\|_{L^2}^2 - \frac{1}{2\Delta t}\sum_{i=b,ts}\left\|\theta_i^{h,n-1}\right\|_{L^2}^2 + \sum_{i=b,ts}\underline{\eta}_i\left\|\theta_i^{h,n}\right\|_{H^1}^2 \\ &- \sum_{i=b,ts}\frac{\underline{\eta}_i}{2}\left\|\theta_i^{h,n}\right\|_{L^2}^2 - C(\underline{\eta}_b, \underline{\eta}_{ts})\sum_{i=b,ts}\left\|\varphi_i^{h,n-1}\right\|_{L^2}^2 + \sum_{i=b,ts}\underline{\sigma}_i\left\|\varphi_i^{h,n}\right\|_{H^1}^2 \\ = &\left(\frac{1}{2\Delta t}\left\|\boldsymbol{u}^{h,n}\right\|_{L^2}^2 + \underline{\nu}\left\|\boldsymbol{u}^{h,n}\right\|_{H^1}^2 + \frac{1}{2\Delta t}\sum_{i=b,ts}\left\|\theta_i^{h,n}\right\|_{L^2}^2 + \sum_{i=b,ts}\frac{\underline{\eta}_i}{2}\left\|\theta_i^{h,n}\right\|_{H^1}^2\right. \\ &\left. + \sum_{i=b,ts}\underline{\sigma}_i\left\|\varphi_i^{h,n}\right\|_{H^1}^2\right) - \left(\frac{1}{4\Delta t}\left\|\boldsymbol{u}^{h,n-1}\right\|_{L^2}^2 + \frac{1}{2\Delta t}\sum_{i=b,ts}\left\|\theta_i^{h,n-1}\right\|_{L^2}^2\right. \\ &\left. + C(\underline{\eta}_b, \underline{\eta}_{ts})\sum_{i=b,ts}\left\|\varphi_i^{h,n-1}\right\|_{L^2}^2 + C(\Delta t)\left\|\boldsymbol{F}^{h,n}\right\|_{L^2}^2\right) \\ \ge &\min\left\{\frac{1}{2\Delta t}, \underline{\nu}, \frac{1}{2\Delta t}, \frac{\underline{\eta}_b}{2}, \frac{\underline{\eta}_{t,s}}{2}, \underline{\sigma}_b, \underline{\sigma}_{ts}\right\}\left\|Y^{h,n}\right\|_{E_h}^2 - \left(\frac{1}{4\Delta t}\left\|\boldsymbol{u}^{h,n-1}\right\|_{L^2}^2\right. \\ &\left. + \frac{1}{2\Delta t}\sum_{i=b,ts}\left\|\theta_i^{h,n-1}\right\|_{L^2}^2 + C(\underline{\eta}_b, \underline{\eta}_{ts})\sum_{i=b,ts}\left\|\varphi_i^{h,n-1}\right\|_{L^2}^2 + C(\Delta t)\left\|\boldsymbol{F}^{h,n}\right\|_{L^2}^2\right).\end{aligned} \tag{66}$$

Finally for a given $\boldsymbol{u}^{h,n-1}$, $\theta_i^{h,n-1}$ and $\varphi_i^{h,n-1}$, we deduce from (66) that (65) holds for r large enough (recall that $\left\|Y^{h,n}\right\|_{E_h} = r$) for $i = b, ts$. Hence, we obtain the existence of at least one solution to the discrete finite element scheme (64). ■

Remark 4.1. *Although the convergence proof of the finite element solution* $\mathbf{U}^h = \left(\boldsymbol{u}^h, \theta_b^h, \theta_{ts}^h, \varphi_b^h, \varphi_{ts}^h\right)$*, generated by* (64)*, is postponed to [7], let us indicate its main steps. The convergence of the discrete solution* $\mathbf{U}^h$ *to* $\mathbf{U} = \left(\boldsymbol{u}, \theta_b, \theta_{ts}, \varphi_b, \varphi_{ts}\right)$ *(where* $\mathbf{U}$ *is a weak solution in the sense of Definition 2.1) can then be proved (see [7] for more details) by passing to the limit* $h \to 0$ *in a sequence* $\mathbf{U}^h$ *satisfying the following numerical stability (discrete energy estimates)*

$$\begin{aligned}
&\left\|\boldsymbol{u}^h\right\|_{L^\infty(0,T;L^2(\Omega_b))} + \left\|\nabla \boldsymbol{u}^h\right\|_{L^2(\Omega_{T,b},\mathbb{R}^3)} \leq C,\\
&\sum_{i=b,ts} \left\|\varphi_i^h\right\|_{L^\infty(\Omega_{T,i})} + \sum_{i=b,ts} \left\|\nabla \varphi_i^h\right\|_{L^2(\Omega_{T,i})} \leq C,\\
&\sum_{i=b,ts} \left\|\theta_i^h\right\|_{L^\infty(0,T;L^2(\Omega_i))} + \sum_{i=b,ts} \left\|\nabla \theta_i^h\right\|_{L^2(\Omega_{T,i})} \leq C,
\end{aligned} \tag{67}$$

for some constant $C > 0$ *not depending on* h*. Next, we derive the following estimates on differences of space and time translates of the function* $\mathbf{W}^h := \boldsymbol{u}^h,\ \theta_b^h, \theta_{ts}^h$*:*

$$\begin{aligned}
&\iint_{\Omega_b' \times (0,T)} \left|\boldsymbol{u}^h(t, x+r) - \boldsymbol{u}^h(t,x)\right|^2 dxdt + \sum_{i=b,ts} \iint_{\Omega_i' \times (0,T)} \left|\theta_i^h(t, x+r) - \theta_i^h(t,x)\right|^2 dxdt\\
&\qquad \leq C\,|r|^2 + T \sup_{0<|r|\leq\delta} \int_{\Omega_b'} |\boldsymbol{u}_0^h(x+r) - \boldsymbol{u}_0^h(x)|^2 dx + T \sup_{0<|r|\leq\delta} \sum_{i=b,ts} \int_{\Omega_i'} |\theta_{i,0}^h(x+r) - \theta_{i,0}^h(x)|^2 dx,
\end{aligned} \tag{68}$$

for all $r \in \mathbb{R}^3$ *with* $\Omega_i' = \{x \in \Omega_i,\ [x, x+r] \subset \Omega_i\}$ *for* $i = b, ts$*, and*

$$\iint_{\Omega_b \times (0,T-\tau)} \left|\boldsymbol{u}^h(t+\tau, x) - \boldsymbol{u}^h(t,x)\right|^2 dxdt + \sum_{i=b,ts} \iint_{\Omega_i \times (0,T-\tau)} \left|\theta_i^h(t+\tau, x) - \theta_i^h(t,x)\right|^2 dxdt \leq C(\tau + \Delta t) \tag{69}$$

for all $\tau \in (0,T)$*, for some constant* $C > 0$*.*
The consequence of (68)*,* (69)*,* (67) *and Kolmogorov's compactness criterion yield the following convergences*

$$\begin{aligned}
&\boldsymbol{u}^h \to \boldsymbol{u} \text{ strongly in } L^2(\Omega_{T,b}) \text{ and a.e. in } \Omega_{T,b},\\
&\theta_i^h \to \theta_i \text{ strongly in } L^2(\Omega_{T,i}) \text{ and a.e. in } \Omega_{T,i},\\
&\boldsymbol{u}^h \rightharpoonup \boldsymbol{u} \text{ weakly in } L^2(0,T; H^1(\Omega_b)),\\
&\theta_i^h \rightharpoonup \theta_i \text{ weakly in } L^2(0,T; H^1(\Omega_i)),\\
&\varphi_i^h \rightharpoonup \varphi_i \text{ weakly in } L^2(0,T; H^1(\Omega_i)),
\end{aligned} \tag{70}$$

for $i = b, ts$*. Exploiting the convergence* (70)*, we can send* $h \to 0$ *in* (64) *to conclude that the limit* $\mathbf{U} = \left(\boldsymbol{u}, \theta_b, \theta_{ts}, \varphi_b, \varphi_{ts}\right)$ *is a weak solution in the sense of Definition 2.1.*

4.2. Numerical results

First, we mention here an interesting question which is how to treat the temperature advection-diffusion equation. Obviously, not all discretization of this equation are equally stable without regularization techniques. For this reason, we can use discontinuous elements which is more efficient for pure advection problems. However, in the presence of diffusion terms, the discretization of the Laplace operator is cumbersome due to the large number of additional terms that must be integrated on each face between the cells. Consequently, a better alternative is to add some nonlinear viscosity $\tilde{\eta}(\theta)$ to the model that only acts in the vicinity of shocks and other discontinuities. The viscosity $\tilde{\eta}(\theta)$ is chosen in such a way that if θ satisfies the original equations, the additional viscosity is zero. In our case, we will opt

for the stabilization strategy developed in [21] that builds on a suitably defined residual and a limiting procedure for the additional viscosity. For this, let us define a residual $R_\alpha(\theta)$ as follows:

$$R_\alpha(\theta) = \left(\frac{\partial\theta}{\partial t} + \mathbf{u}\cdot\nabla\theta - \nabla\cdot\eta\left(\bar{\theta}\right)\nabla\theta - \sigma\left(\bar{\theta}\right)|\nabla\varphi|^2\right)\theta^{\alpha-1}, \quad \alpha\in[1,2].$$

Note that $R_\alpha(\theta)$ will be zero if θ satisfies the temperature equation. Multiplying terms out, we obtain the following entirely equivalent form:

$$R_\alpha(\theta) = \frac{1}{\alpha}\frac{\partial(\theta^\alpha)}{\partial t} + \frac{1}{\alpha}\mathbf{u}\cdot\nabla(\theta^\alpha) - \frac{1}{\alpha}\nabla\cdot\eta\left(\bar{\theta}\right)\nabla(\theta^\alpha) + \eta\left(\bar{\theta}\right)(\alpha-1)\theta^{\alpha-2}|\nabla\theta|^2 - \gamma\theta^{\alpha-1}.$$

Using the above equation, we define the artificial viscosity as a piece-wise constant function defined on each cell K with diameter h_K separately giving by:

$$\tilde{\eta}_\alpha(\theta)\big|_K = \beta\|\mathbf{u}\|_{L^\infty(K)}\min\left\{h_K, h_K^\alpha\frac{\|R_\alpha(\theta)\|_{L^\infty(K)}}{c(\mathbf{u},\theta)}\right\},$$

where, β is a stabilization constant and $c(\mathbf{u},\theta) = c_R\|\mathbf{u}\|_{L^\infty(\Omega)}\,\mathrm{var}(\theta)\,|\,\mathrm{diam}(\Omega)\,|^{\alpha-2}$ where $\mathrm{var}(\theta) = \max_\Omega\theta - \min_\Omega\theta$ is the range of present temperature values and c_R is a dimensionless constant.
If on a particular cell the temperature field is smooth, then we expect the residual to be small and the stabilization term that injects the artificial diffusion will be rather small, when no additional diffusion is needed. In addition, if we are on or near a discontinuity in the temperature field, then the residual will be large and the artificial viscosity will ensure the stability of the scheme.

Our goal is to show that the proposed model can reproduce the very interesting characteristics and phenomena of radiofrequency ablation. In particular, we demonstrate the influence of electrical potential in cardiac tissue, saline viscosity and external forces. Numerical results are provided based on existing parameters in the literature, for instance, [18, 19, 20]. We consider a Ω domain which is decomposed by two sub-domains Ω_b and Ω_{ts} as described in Figure 2 where $L = 1.5$, $H = 1$ and $r = 0.075$. In our numerical simulations, the electrode thickness is assumed negligible because their diameter is very small. However, the numerical simulation in three-dimensional space with the optimal control will be studied in our next work. In addition, the electrical conductivities σ_i, thermals conductivities η_i, and blood conductivity ν have been modeled as temperature-dependent functions and are given by the following equations

$$\begin{aligned}
\sigma_b(\theta_b) &= \begin{cases} \sigma_0\exp\left(0.015\left(\theta_b-\bar{\theta}\right)\right) & \text{for } \theta_b \le 99°\text{C},\\ 2.5345\sigma_0 & \text{for } 99°\text{C} < \theta_b \le 100°\text{C},\\ 2.5345\sigma_0\left(1-0.198\left(\theta_b-100°\text{C}\right)\right) & \text{for } 100°\text{C} < \theta_b \le 105°\text{C},\\ 0.025345\sigma_0 & \text{for } \theta_b > 105°\text{C}, \end{cases}\\
\eta_b(\theta_b) &= \begin{cases} \eta_0 + 0.0012\left(\theta_b-\bar{\theta}\right) & \text{for } \theta_b \le 100°\text{C},\\ \eta_0 + 0.0012\left(100°\text{C}-\bar{\theta}\right) & \text{for } \theta_b > 100°\text{C}, \end{cases}\\
\sigma_{ts}(\theta_{ts}) &= \sigma_0 + 0.02\left(\theta_{ts}-\bar{\theta}\right),\\
\eta_{ts}(\theta_{ts}) &= \eta_0 + 0.0012\left(\theta_{ts}-\bar{\theta}\right),
\end{aligned}$$

where $\sigma_0 = 0.6$ and $\eta_0 = 0.54$ are the constant electrical conductivity and the thermal conductivity, respectively, at core body temperature, $\bar{\theta} = 37°\text{C}$ and $\varphi_d = 1$. Moreover, the viscosity and density of blood are 0.0021 Pa · s and 1000 kg/m^3, respectively, while those of saline are 0.001 Pa · s and 1000 kg/m^3, respectively, based on the material property of water.

Finally, we consider the following boundary conditions. A velocity $\boldsymbol{u} = \boldsymbol{u}_e = \begin{pmatrix} 4y(H-y) \\ 0 \end{pmatrix}$ on boundary Σ_1, $\boldsymbol{u} = \boldsymbol{u}_s$ on boundary Σ_8, and we change the boundary condition of the viscosity in the boundary Σ_3 that is $-\pi\boldsymbol{n}_b + \nu\left(\theta_b\right)\mathbb{D}(\boldsymbol{u})\boldsymbol{n}_b = \boldsymbol{0}$. On boundaries Σ_i, $i = 2, 7$, we assume that the velocity is zero i.e., $\boldsymbol{u} = \begin{pmatrix} 0 \\ 0 \end{pmatrix}$ on $\Sigma_2\cup\Sigma_7$. We set on the boundaries Σ_i, $i = 1,\cdots,6$ the temperatures, $\theta_b = \theta_{ts} = 37°\text{C}$. For the potential equation, we fix $\varphi_i = \varphi_d = 1$ on Σ_8 and the homogeneous Dirichlet condition in the remaining boundaries. In the following, we provide three numerical experiments where the aims are to show the influences of the saline flow and the external force.

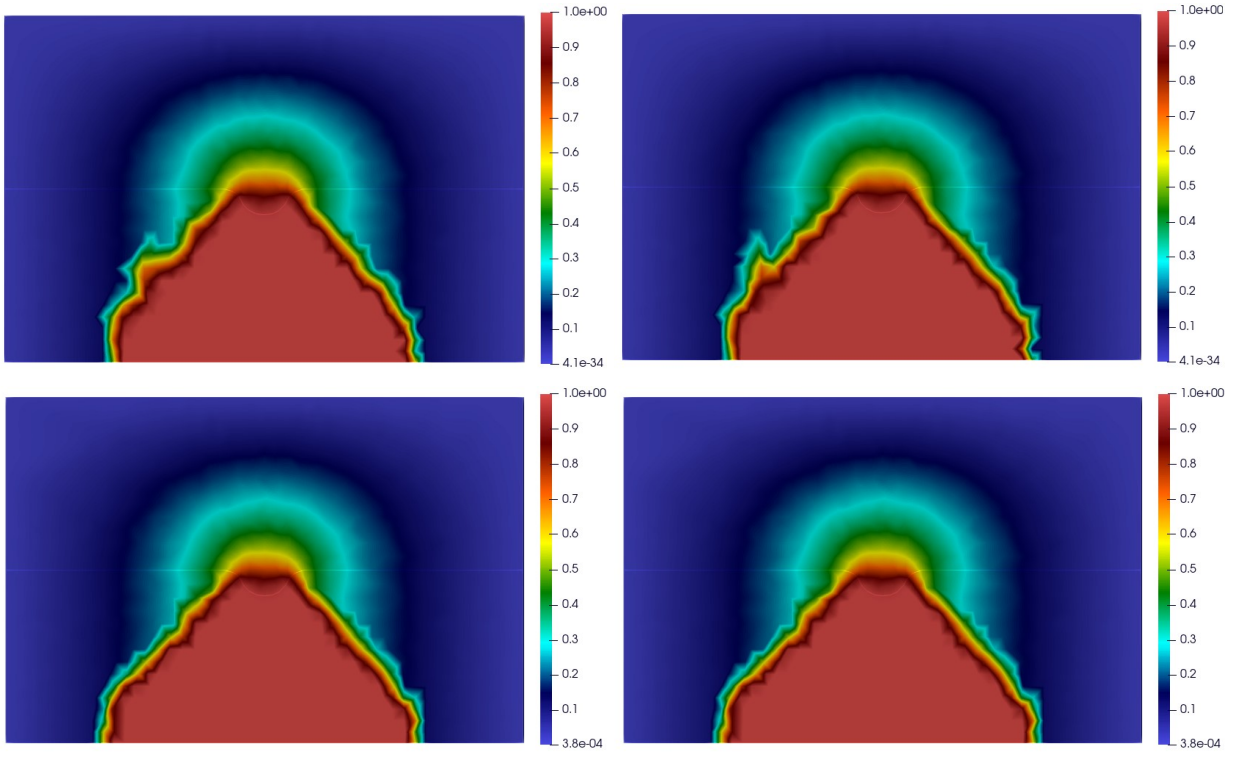

Figure 3: Snapshot of evolution of the potentials at four time moments $t = \frac{T}{6}, \frac{T}{2}, \frac{3T}{4}, T$.

4.2.1. Test 1: heat transfer and blood flow

The aim of this test is to show that our model is validated by comparing with the results from the literature. First of all, we mention that the impact of saline viscosity and the external forces are neglected, which is expressed as $\boldsymbol{u}_s = 0$ and $\mathbf{F} = 0$. In this scenario, the continuity condition is used in place of the saline heat and the Dirichlet condition of viscosity on the boundary of Σ_3, which are $\left(\eta_b\left(\theta_b\right)\nabla\theta_b\right)\cdot\boldsymbol{n}_b = -\left(\eta_{ts}\left(\theta_{ts}\right)\nabla\theta_{ts}\right)\cdot\boldsymbol{n}_b$ on Σ_8 and $\boldsymbol{u} = \boldsymbol{u}_e$ on Σ_3, respectively.

The first remark is that the computed potential evolves very slowly during the time iterations, see Figure 3. This can be justified by the fact that the only data in the potential equation is the source φ_i which is constant and the electrical conductivity σ_i. Thus, we omit the figures of the potential as there is no significant change during the iterations.

Now, let comment on the mechanism of how and why we got our numerical results. The applied potential increases the temperature of the tissue part near to the catheter and then diffusing in cardiac tissue domain, see Figure 4. Thanks to the the continuity on the boundaries, the temperature of the blood domain is also increased, this can be justified by the presence of the electric field term $-\sigma_{ts}\left(\theta_{ts}\right)\nabla\varphi_{ts}\cdot\nabla\varphi_{ts}$. It is important to mention that this temperature is also influenced by the presence of the blood. More precisely, it is transported in the direction of the fluid because of the presence of the term $\boldsymbol{u}\cdot\nabla\theta_b$. On the other hand, it is clear that the speed of the fluid and the pressure in the fluid part are influenced by the viscosity which depends on the temperature θ_b. More precisely, we see a flow recirculation zone, with a local enhance of velocity upstream to the catheter. While it remains almost uniform in the other regions far from the catheter at time $T/6$. In time progress, we can see that the velocity and the pressure are influenced by the presence of the viscosity, see the second column of Figure 4.

To cut it short, this test shows the influence of each term in our model, it shows the coupling effects, that is to say, the fluid, the pressure, the temperatures, and the potentials are affecting each other.

There is close agreement between the model and the experimental results from the literature.

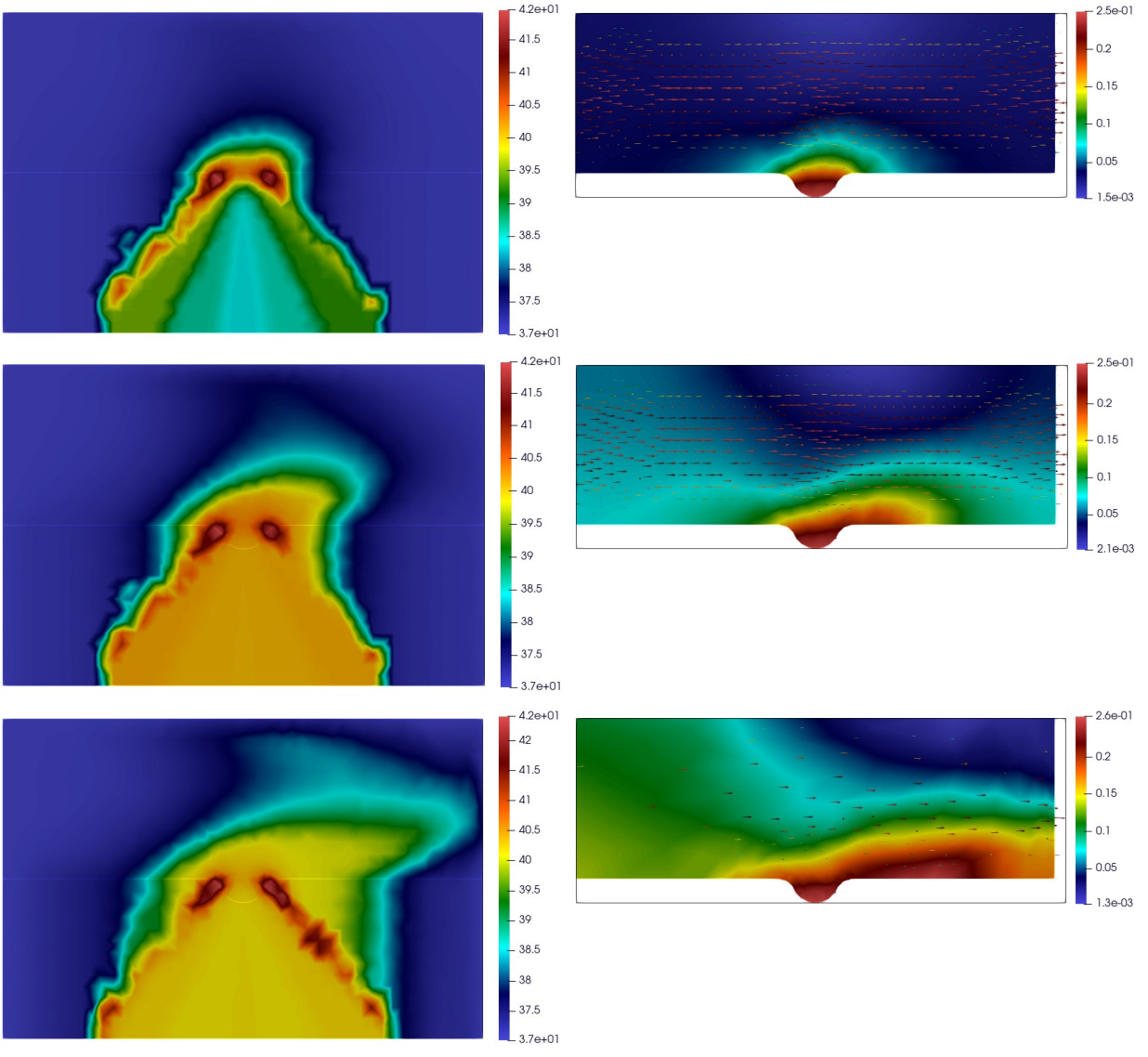

Figure 4: Test 1 : evolution of heats (column 1), velocity and pressure (column 2) at three time moments $t = \frac{T}{6}$ (line 1), $t = \frac{T}{2}$ (line 2) and $t = T$ (line 3).

4.2.2. Test 2: the saline flow effect

In this test, we aim to demonstrate the effect of the saline flow. As it is shown in Test 1 (cf. Subsection 4.2.1), the temperature in the neighborhoods of the catheter achieves a critical values between 40°C and 42°C. Thus, naturally it is necessary to cool down this zone and make it's temperature down. For that, we need to inject a fluid where the saline heat is 20°C i.e., $\theta_b = \theta_{ts} = \theta_s = 20°C$ on Σ_8. This can be done by considering the following $\boldsymbol{u} = \boldsymbol{u}_s = \begin{pmatrix} \frac{20}{r}\left(x - \frac{L}{2} + r\right)\left(\frac{L}{2} + r - x\right)\left(\frac{L}{2} - x\right) \\ \frac{-20}{r}\left(x - \frac{L}{2} + r\right)\left(\frac{L}{2} + r - x\right) y \end{pmatrix}$, on boundary Σ_8. To present these evolution, we show in Figure 5 the results of numerical simulations at three different times $t = \frac{T}{6}, \frac{T}{2}, T$, where each row of the figure represents the corresponding time in the same order. In the first column, we show the heats θ_b and θ_{ts}, and in the second column, we show the velocity field and the pressure. Clearly, we notice that the injected saline flow $\mathbf{u}_s$ diminishes the calculated heats. This leads to the possibility of cooling the domain by the saline fluid from Σ_8. In addition, we observe the

rotation of the fluid in the areas subject to heat variations, especially in the area near the outlet boundary Σ_3.

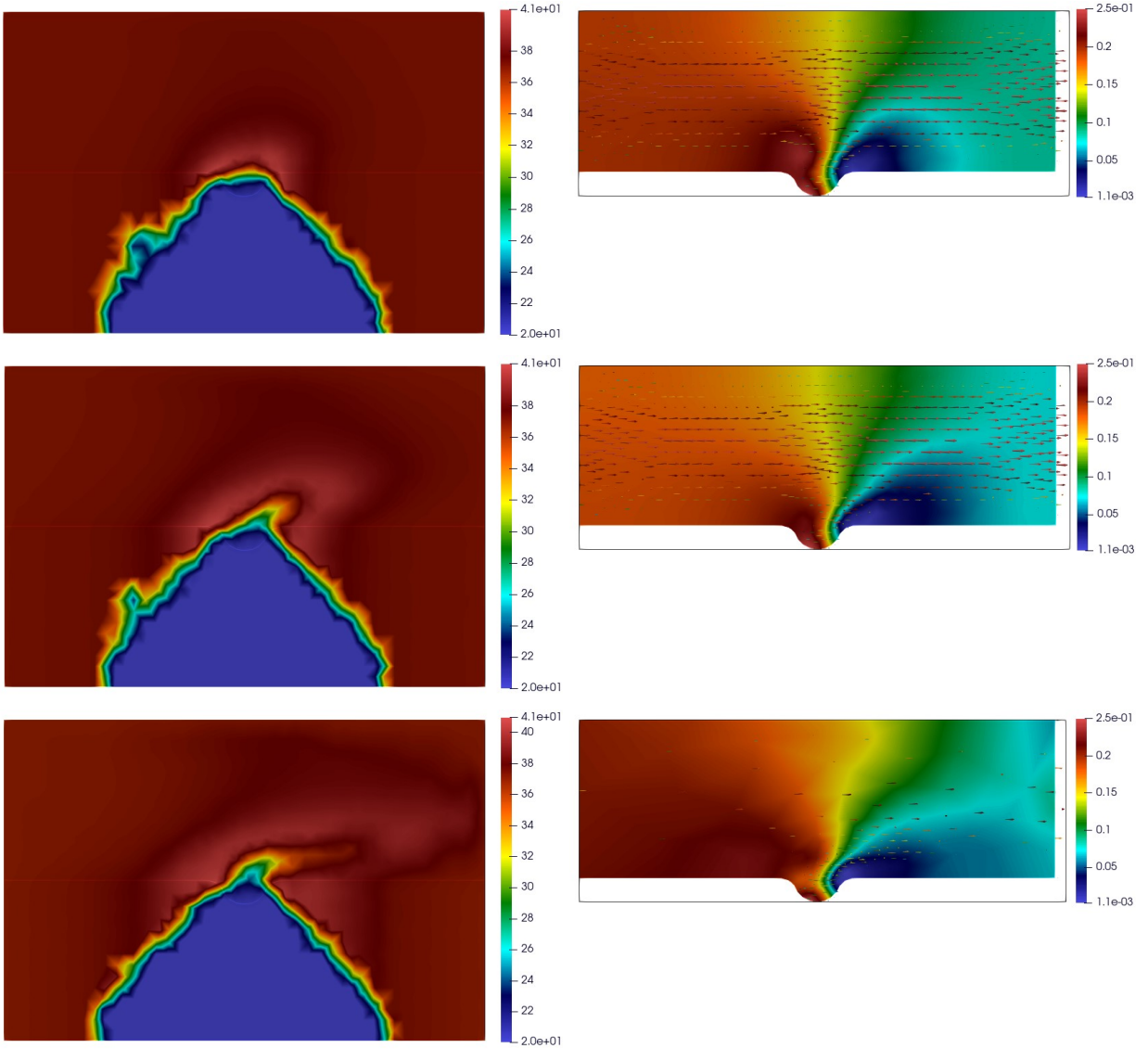

Figure 5: Test 2 : evolution of heats (column 1), velocity and pressure (column 2) at three time moments $t = \frac{T}{6}$ (line 1), $t = \frac{T}{2}$ (line 2) and $t = T$ (line 3).

4.2.3. Test 3: the external force effect

In final test, we are interested in the behavior of the heats when the fluid source term is non-zero. Thus, we consider the fluid source $\mathbf{F} = -\begin{pmatrix} 0 \\ 10^{-3}9.81/303\,(\theta_b - \bar{\theta}) \end{pmatrix}$ as in Boussinesq equations. Figure 6 represents the evolution of the heats θ_i (first column) and of the velocity and pressure (column 2) at times $t = \frac{T}{6}, \frac{T}{2}$, and T. We notice the rotation of the fluid in the areas subject to heat variations, especially in the area near the outlet boundary Σ_3. This is justified by the structure of the source term $\mathbf{F}$, in particular the term $\theta_b - \bar{\theta}$. Indeed by the principle of maximum, the velocity changes its sign according to the value of the temperature θ_b whether it is lower or higher than $\bar{\theta}$. Consequently, we achieve a reduction of the temperature in certain areas of the domain.

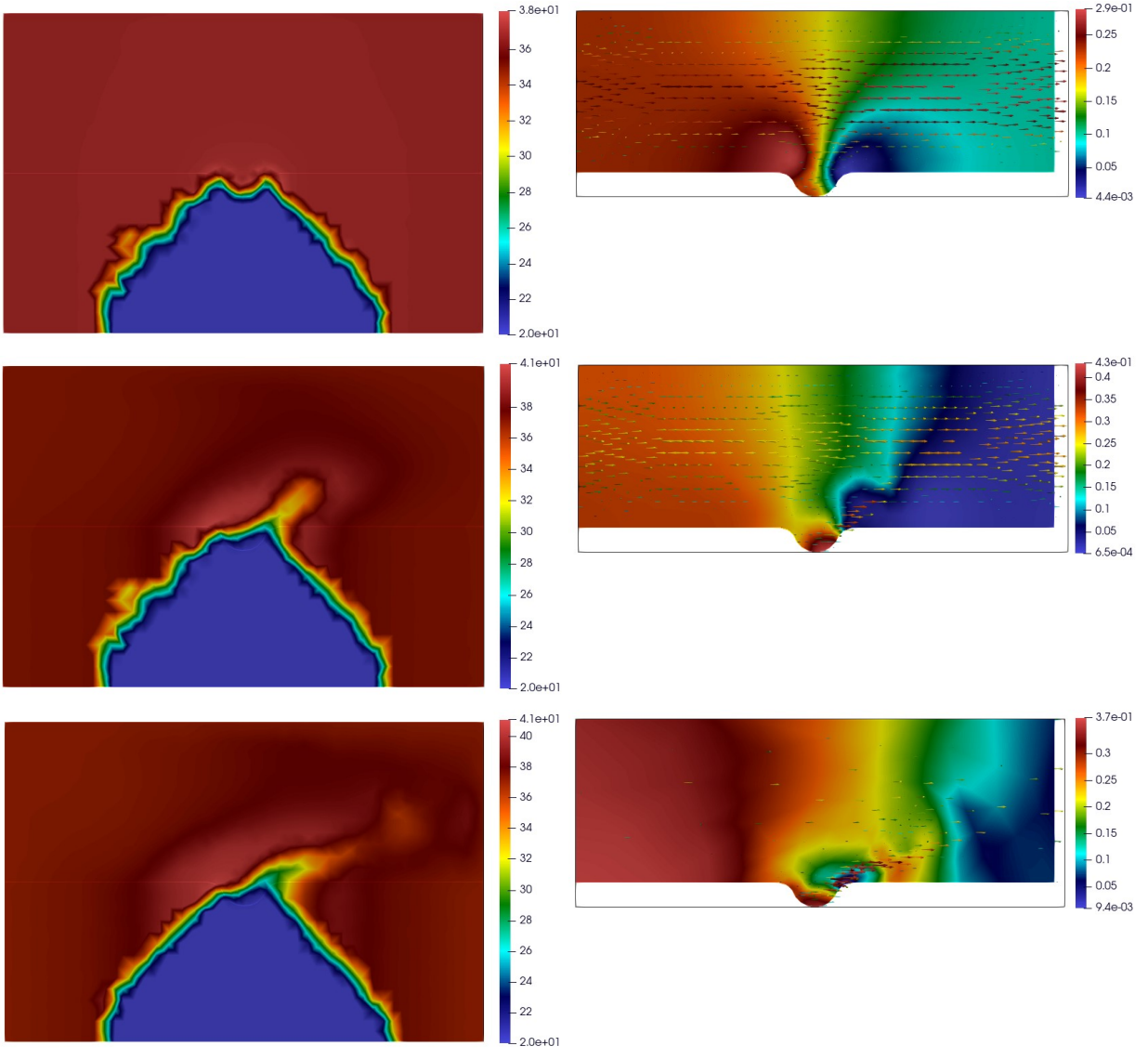

Figure 6: Test 3 : evolution of heat (column 1), velocity and pressure (column 2) at three time moments $t = 0$ (line 1), $t = \frac{T}{2}$ (line 2) and $t = T$ (line 3).

5. Conclusion and perspectives

In this paper, a new coupled electro-thermo-fluid RFA model describing radiofrequency ablation phenomena in cardiac tissue and Newtonian fluid medium governed by the incompressible Navier–Stokes has been proposed. The proposed model can be considered as an improved model in [8]. Indeed, their model consists of a coupled thermistor and the incompressible Navier–Stokes equations that describe the evolution of temperature, velocity, and potential only in the blood vessel.

In this work, the existence of weak solutions has been proved using the Faedo–Galerkin with a priori estimates and compactness arguments. In addition, numerical simulations in different cases have been illustrated in a two-dimensional space using the finite element method.

Our proposed model can be considered as a general mathematical framework that is capable of including the following features: a radiofrequency ablation phenomenon for cardiac tissue, predicting the temperature of the tissues, the saline flow, and the external force. These features are demonstrated in our numerical simulations. We believe this

work can lead to interesting perspectives, such as optimal control models and inverse problems, namely the identification of the frequency factor of different tissue types. In addition, other perspectives consist of studying the optimal control of the proposed model and improving it by adding the stochastic effects, for instance in the incompressible Navier–Stokes equation, see [7, 5].

References

[1] Adams, Robert A et Fournier, J., 2003. Espaces de Sobolev mathématiques pures et appliquées (amsterdam), 140.

[2] Akrivis, G., Larsson, S., 2005. Linearly implicit finite element methods for the time-dependent Joule heating problem. BIT Numerical Mathematics 45, 429–442.

[3] Allegretto, W., Xie, H., 1992. Existence of solutions for the time-dependent thermistor equations. IMA Journal of Applied Mathematics 48, 271–281.

[4] Antontsev, S., Chipot, M.M., 1994. The thermistor problem: existence, smoothness uniqueness, blowup. SIAM Journal on Mathematical Analysis 25, 1128–1156.

[5] Bendahmane, M., Jacques, T., Zagour, M., 2022. Odd-Even based asymptotic preserving scheme for a 2D stochastic kinetic-fluid model. J. Comput. Phys. 471, Paper No. 111649, 25.

[6] Bendahmane, M., Mroue, F., Saad, M., Talhouk, R., 2019. Unfolding homogenization method applied to physiological and phenomenological bidomain models in electrocardiology. Nonlinear Analysis: Real World Applications 50, 413–447.

[7] Bendahmane, M., Ouakrim, Y., Ouzrour, Y., Zagour, M., 2024a. Numerical analysis of a finite element method for an optimal control of a coupled electro-thermo radiofrequency model of cardiac tissue. Preprint .

[8] Bendahmane, M., Ouakrim, Y., Ouzrour, Y., Zagour, M., 2024b. Toward fluid radiofrequency ablation of cardiac tissue: modeling, analysis and simulations. Preprint under review, Arxiv.org/abs/2312.09965.

[9] Berjano, E.J., 2006. Theoretical modeling for radiofrequency ablation: state-of-the-art and challenges for the future. Biomedical engineering online 5, 1–17.

[10] Bernardi, C., Dib, S., Girault, V., Hecht, F., Murat, F., Sayah, T., 2018. Finite element methods for Darcy's problem coupled with the heat equation. Numerische Mathematik 139, 315–348.

[11] Brezis, H., 1983. Analyse fonctionnelle. théorie et applications. collection mathématiques appliquées pour la maıtrise.

[12] Cimatti, G., 1992. Existence of weak solutions for the nonstationary problem of the Joule heating of a conductor. Annali di Matematica pura ed applicata 162, 33–42.

[13] Fang, Z., Wei, H., Zhang, H., Moser, M.A., Zhang, W., Qian, Z., Zhang, B., 2022. Radiofrequency ablation for liver tumors abutting complex blood vessel structures: treatment protocol optimization using response surface method and computer modeling. International Journal of Hyperthermia 39, 733–742.

[14] Formaggia, L., Quarteroni, A., Veneziani, A., 2009. Cardiovascular mathematics, volume 1 of MS&A. modeling, simulation and applications.

[15] Fouchet-Incaux, J., 2014. Artificial boundaries and formulations for the incompressible navier–stokes equations: applications to air and blood flows. SeMA Journal 64, 1–40.

[16] Franck, B., Pierre, F., 2012. Mathematical Tools for the Study of the Incompressible Navier–Stokes Equations and Related Models. volume 183. Springer Science & Business Media.

[17] Gao, H., 2016. Unconditional optimal error estimates of BDF-Galerkin FEMs for nonlinear thermistor equations. Journal of Scientific Computing 66, 504–527.

[18] González-Suárez, A., Berjano, E., 2015. Comparative analysis of different methods of modeling the thermal effect of circulating blood flow during RF cardiac ablation. IEEE Transactions on Biomedical Engineering 63, 250–259.

[19] González-Suárez, A., Berjano, E., Guerra, J.M., Gerardo-Giorda, L., 2016. Computational modeling of open-irrigated electrodes for radiofrequency cardiac ablation including blood motion-saline flow interaction. PloS one 11, e0150356.

[20] González-Suárez, A., Pérez, J.J., Berjano, E., 2018. Should fluid dynamics be included in computer models of RF cardiac ablation by irrigated-tip electrodes? Biomedical engineering online 17, 1–14.

[21] Guermond, J.L., Pasquetti, R., Popov, B., 2011. Entropy viscosity method for nonlinear conservation laws. Journal of Computational Physics 230, 4248–4267.

[22] Haemmerich, D., 2010. Mathematical modeling of impedance controlled radiofrequency tumor ablation and ex-vivo validation, in: 2010 Annual International Conference of the IEEE Engineering in Medicine and Biology, IEEE. pp. 1605–1608.

[23] Huaman, D.N., Nuñez-Chávez, M.R., Límaco, J., Carvalho, P.P., 2023. Local null controllability for the thermistor problem. Nonlinear Analysis , 113330.

[24] Johnson, P.C., Saidel, G.M., 2002. Thermal model for fast simulation during magnetic resonance imaging guidance of radio frequency tumor ablation. Annals of Biomedical Engineering 30, 1152–1161.

[25] Li, B., Gao, H., Sun, W., 2014. Unconditionally optimal error estimates of a Crank–Nicolson Galerkin method for the nonlinear thermistor equations. SIAM Journal on Numerical Analysis 52, 933–954.

[26] Li, B., Sun, W., 2013. Error analysis of linearized semi-implicit Galerkin finite element methods for nonlinear parabolic equations. Int. J. Numer. Anal. Mod. 10, 622–633.

[27] Li, B., Yang, C., 2015. Uniform BMO estimate of parabolic equations and global well-posedness of the thermistor problem, in: Forum of Mathematics, Sigma, Cambridge University Press.

[28] Linte, C.A., Camp, J.J., Rettmann, M.E., Haemmerich, D., Aktas, M.K., Huang, D.T., Packer, D.L., Holmes III, D.R., 2018. Lesion modeling, characterization, and visualization for image-guided cardiac ablation therapy monitoring. Journal of Medical Imaging 5, 021218–021218.

[29] Meinlschmidt, H., Meyer, C., Rehberg, J., 2017a. Optimal control of the thermistor problem in three spatial dimensions, part 1: Existence of

optimal solutions. SIAM Journal on Control and Optimization 55, 2876–2904.

[30] Meinlschmidt, H., Meyer, C., Rehberg, J., 2017b. Optimal control of the thermistor problem in three spatial dimensions, part 2: Optimality conditions. SIAM Journal on Control and Optimization 55, 2368–2392.

[31] Petras, A., Leoni, M., Guerra, J.M., Jansson, J., Gerardo-Giorda, L., 2019. A computational model of open-irrigated radiofrequency catheter ablation accounting for mechanical properties of the cardiac tissue. International Journal for Numerical Methods in Biomedical Engineering 35, e3232.

[32] Quarteroni, A., Manzoni, A., Vergara, C., 2017. The cardiovascular system: mathematical modelling, numerical algorithms and clinical applications. Acta Numerica 26, 365–590.

[33] Roger, T., 2001. Navier–Stokes Equations: Theory and Numerical Analysis, 3rd edition. reprinted in AMS Chelsea series by American Mathematical Society, Providence, North-Holland, Amsterdam.

[34] Salhi, L., Seaid, M., Yakoubi, D., 2022. Well-posedness and numerical approximation of steady convection-diffusion-reaction problems in porous media. Computers & Mathematics with Applications 124, 129–148.

[35] Sánchez-Muñoz, E.J., Berjano, E., González-Suárez, A., 2022. Computer simulations of consecutive radiofrequency pulses applied at the same point during cardiac catheter ablation: Implications for lesion size and risk of overheating. Computer methods and programs in biomedicine 220, 106817.

[36] Vaidya, N., Baragona, M., Lavezzo, V., Maessen, R., Veroy, K., 2021. Simulation study of the cooling effect of blood vessels and blood coagulation in hepatic radio-frequency ablation. International Journal of Hyperthermia 38, 95–104.

[37] Villard, C., Soler, L., Gangi, A., 2005. Radiofrequency ablation of hepatic tumors: simulation, planning, and contribution of virtual reality and haptics. Computer Methods in Biomechanics and Biomedical Engineering 8, 215–227.

[38] Yuan, G., Liu, Z., 1994. Existence and uniqueness of the C^{α}-solution for the thermistor problem with mixed boundary value. SIAM Journal on Mathematical Analysis 25, 1157–1166.

[39] Zhang, B., Moser, M.A., Zhang, E.M., Luo, Y., Liu, C., Zhang, W., 2016. A review of radiofrequency ablation: Large target tissue necrosis and mathematical modelling. Physica Medica 32, 961–971.